A preclinical trial and molecularly-annotated patient cohort identify predictive biomarkers in homologous recombination deficient pancreatic cancer

A preclinical trial and molecularly-annotated patient cohort identify predictive biomarkers in homologous recombination deficient pancreatic cancer

Yifan Wang[1,2], Jin Yong Patrick Park[1,2], Alain Pacis[1,3], Robert E. Denroche[4], Gun Ho Jang[4], Amy Zhang[4], Adeline Cuggia[1,2], Celine Domecq[1,2], Jean Monlong[5], Maria Raitses-Gurevich[6], Robert C. Grant[4,8], Ayelet Borgida[9], Spring Holter[9], Chani Stossel[6,7], Simeng Bu[1,2], Mehdi Masoomian[10], Ilinca Lungu[4], John Bartlett[4,10], Julie M. Wilson[4], Zu-Hua Gao[11], Yasser Riazalhosseini[5], Jamil Asselah[12], Nathaniel Bouganim[12], Tatiana Cabrera[13], Louis-Martin Boucher[13], David Valenti[13], James Biagi[14], Celia M.T. Greenwood[5,12,15,16], Paz Polak[17], William D. Foulkes[2,5], Talia Golan[6,7], Grainne M. O'Kane[4,8], Sandra E. Fischer[10], Jennifer J. Knox[8], Steven Gallinger[4,8], George Zogopoulos[1,2]*

Short Title: Predictive biomarkers in HRD pancreatic cancer

Affiliations

[1]Rosalind and Morris Goodman Cancer Research Centre of McGill University, Montreal, QC, Canada.

[2]Research Institute of the McGill University Health Centre, Montreal, QC, Canada.

[3]Canadian Centre for Computational Genomics, McGill University and Genome Quebec Innovation Center, Montreal, QC, Canada.

[4]Ontario Institute for Cancer Research, Toronto, ON, Canada.

[5]Department of Human Genetics, McGill University, Montreal, QC, Canada.

[6]Pancreatic Cancer Translational Research Laboratory, Oncology Institute, Sheba Medical Center, Tel Hashomer, Israel.

[7]Sackler Faculty of Medicine, Tel Aviv University, Tel Aviv, Israel.

[8]Wallace McCain Centre for Pancreatic Cancer, Princess Margaret Cancer Centre, Toronto, ON, Canada.

[9]Lunenfeld Tanenbaum Research Institute, Mount Sinai Hospital, Toronto, ON, Canada.

[10]Department of Laboratory Medicine and Pathobiology, University of Toronto, Toronto, ON, Canada.

[11]Department of Pathology, McGill University, Montreal, QC, Canada.

[12]Department of Oncology, McGill University, Montreal, QC, Canada.

[13]Department of Diagnostic Radiology, McGill University, Montreal, QC, Canada.

[14]Department of Oncology, Queen's University, Kingston, ON, Canada.

[15]Department of Epidemiology, Biostatistics and Occupational Health, McGill University, Montreal, QC, Canada.

[16]Lady Davis Institute for Medical Research, Jewish General Hospital, Montreal, QC, Canada.

[17]Icahn School of Medicine at Mount Sinai Hospital, New York, NY, USA.

***Corresponding Author:**

George Zogopoulos MD, PhD

McGill University Health Centre

1001 Decarie Blvd, Room EM2.3010

Montreal, Quebec, Canada H4A 3J1

Email: george.zogopoulos@mcgill.ca

Phone: +1(514) 934-1934 #76333

Disclosure of potential competing interests

Talia Golan:

Receipt of grants/research supports: Astra Zeneca and MSD Merck.

Receipt of honoraria or consultation fees: Abbvie, BioLineRx, MSD Merck, Bayer, Teva

Jennifer J. Knox:

Consulting or advisory role: Merck, BMS, Pfizer

Grant and research support: Merck, Pfizer, Astra Zeneca, Ibsen

All other authors have no conflicts of interest to disclose.

Statement of Translational Relevance

Pancreatic cancers associated with a germline *BRCA1*/*BRCA2* (g*BRCA*) mutation may be targetable using DNA-damaging agents, such as platinums and PARP inhibitors. However, treatment stratification based on germline mutational status alone, and assumed homologous recombination deficiency, is associated with heterogeneous outcomes. In this study, we combine a multi-institutional patient cohort and a multi-arm preclinical trial to identify biomarkers to guide treatment decisions. We propose a predictive and prognostic model of g*BRCA*-mutated pancreatic cancer based on genomic hallmarks of homologous recombination deficiency, Ki67 index, tumour ploidy and transcriptomic subtype. Since the basal-like transcriptomic subtype is associated with worse survival, we propose a novel and clinically pragmatic immunohistochemical assay (GATA6:KRT17) to facilitate assignment of transcriptomic subtype.

Abstract

Purpose: Pancreatic ductal adenocarcinoma (PDAC) arising in patients with a germline *BRCA1* or *BRCA2* (g*BRCA*) mutation may be sensitive to platinums and poly(adenosine diphosphate-ribose) polymerase inhibitors (PARPi). However, treatment stratification based on g*BRCA* mutational status alone is associated with heterogeneous responses.

Experimental Design: We performed a 7-arm preclinical trial consisting of 471 mice, representing 12 unique PDAC patient-derived xenografts, of which 9 were g*BRCA*-mutated. From 179 patients whose PDAC was whole genome and transcriptome sequenced, we identified 21 cases with homologous recombination deficiency (HRD), and investigated prognostic biomarkers.

Results: We found that biallelic inactivation of *BRCA1*/*BRCA2* is associated with genomic hallmarks of HRD and required for cisplatin and talazoparib (PARPi) sensitivity. However, HRD genomic hallmarks persisted in xenografts despite the emergence of therapy resistance, indicating the presence of a genomic scar. We identified tumour polyploidy and a low Ki67 index as predictors of poor cisplatin and talazoparib response. In HRD PDAC patients, tumour polyploidy and a basal-like transcriptomic subtype were independent predictors of shorter survival. To facilitate clinical assignment of transcriptomic subtype, we developed a novel pragmatic two-marker assay (GATA6:KRT17).

Conclusions: In summary, we propose a predictive and prognostic model of g*BRCA*-mutated PDAC based on HRD genomic hallmarks, Ki67 index, tumour ploidy and transcriptomic subtype.

Introduction

Pancreatic ductal adenocarcinoma (PDAC) is a difficult-to-treat malignancy with a 9% 5-year overall survival[1,2]. The inefficacy of unselected chemotherapy may reflect the molecular heterogeneity of PDAC. Recently, distinct genomic and transcriptomic subtypes of PDAC have been identified, and may inform treatment stratification[3-6]. 5-10% of incident PDAC cases are associated with germline loss-of-function mutations in *BRCA1*, *BRCA2*, or *PALB2*[7,8]. These genes are implicated in DNA damage response through homologous recombination repair (HRR)[9].

We have previously shown *in vitro* that *BRCA1*- and *BRCA2*-mutated PDAC cell lines are sensitive to platinums and poly(adenosine diphosphate-ribose) polymerase inhibitors (PARPi)[10]. Platinums induce DNA interstrand crosslinks, which lead to double-strand breaks (DSB) that cannot be effectively repaired by homologous recombination deficient (HRD) cells[11]. PARP inhibitors prevent the repair of single-strand breaks (SSB) through several mechanisms, including PARP trapping. As SSBs progress to DSBs, the accumulation of DNA damage is synthetic lethal in replicating HRD cells[12,13].

Retrospective clinical series have suggested that patients with late-stage PDAC and a germline *BRCA1* or *BRCA2* (g*BRCA*) mutation may have a survival benefit with platinum-based treatment[7,14-16]. Recently, the POLO trial showed longer progression-free survival with maintenance olaparib (PARPi) in patients with platinum-sensitive

g*BRCA*-mutated metastatic PDAC[17]. However, 17% of g*BRCA*-mutated patients in this trial progressed on first-line platinum therapy, highlighting the heterogeneity in platinum responses. In g*BRCA*-mutated breast and ovarian cancer, the absence of biallelic *BRCA1* or *BRCA2* inactivation has been implicated in primary resistance to platinum therapy[18]. Reversion mutations that restore *BRCA1* or *BRCA2* function have been described as a mechanism of acquired resistance[19,20]. However, the majority of g*BRCA* tumours do not exhibit a reversion mutation at the time of disease relapse[21]. Together, these observations highlight the need to identify predictive biomarkers, beyond germline mutational status, in g*BRCA*-mutated PDAC.

Here, we performed a multi-arm preclinical trial using mouse xenograft models derived from patients with g*BRCA*-mutated PDAC to evaluate their response to platinum and talazoparib, a second-generation PARPi with speculated higher potency. We demonstrate that HRD genomic hallmarks are required for sensitivity to platinum and PARPi therapy, whereas tumour polyploidy predicts poor response to these therapies. Furthermore, by integrating clinical and molecular profiling data from 21 patients with HRD PDAC, we suggest that tumour polyploidy and a basal-like transcriptomic subtype are poor prognostic variables in HRD PDAC.

Results

1. Biallelic, but not monallelic, BRCA1 or BRCA2 inactivation is associated with genomic hallmarks of HRD

Since biallelic inactivation of *BRCA1* or *BRCA2* has been associated with treatment responses in other cancer types, we whole genome sequenced (WGS) 7 unique g*BRCA*-mutated PDAC cases selected for the preclinical trial (**Supp. Table 1**). Six of the 7 samples showed biallelic loss of *BRCA1* (n = 2) or *BRCA2* (n = 4), due to loss of heterozygosity of the wildtype allele or a second somatic mutation. In contrast, the remaining sample (Q437) exhibited only a germline *BRCA2* mutation without a second somatic hit.

Tumours with biallelic *BRCA1* or *BRCA2* inactivation had higher HRDetect scores compared to the sample with monoallelic loss (>0.999 *vs.* 0.042; **Fig.1a**). Biallelic inactivation cases exhibited a higher number of structural variants, driven by small deletions in the 100bp-10kbp range, consistent with rearrangement signature 5. They also displayed a single nucleotide variant (SNV) burden that was dominated by COSMIC single base substitution signature 3 (SBS3, 32.6% overall SNV), which is associated with defective homologous recombination repair[22]. In contrast, the case with monoallelic *BRCA2* inactivation had 0% SBS3 proportion. These findings suggest that biallelic, but not monoallelic, HR inactivation is associated with distinct mutational

signatures, that are captured by a dominant SBS3 contribution and an elevated HRDetect score.

2. HRD PDAC xenografts are preferentially sensitive to cisplatin and talazoparib mono- and combination therapy

We evaluated 10 unique patient-derived xenografts (PDX) in a multi-arm preclinical trial (387 mice in total) to evaluate their response to platinum, PARPi and gemcitabine-based therapy. Of these 10 PDXs, 6 had biallelic *BRCA1* (n = 2) or *BRCA2* (n = 4) inactivation, and genomic hallmarks of HRD as determined by WGS; these were considered HRD. The remaining xenografts had only monoallelic germline *BRCA2* loss (n = 1) or did not harbour a germline HR gene mutation (n = 3), and were considered HR-proficient (HRP, **Supp. Table 1, Supp. Fig. 1**).

After 28 days of treatment, HRD xenografts showed a significantly greater treatment response to cisplatin monotherapy (2.50 *vs.* 4.97 fold-change, $p < 0.001$), talazoparib monotherapy (2.35 *vs.* 5.73, $p = 0.003$) and cisplatin-talazoparib combination therapy (1.46 *vs.* 4.19, $p < 0.001$) compared to HRP xenografts (**Fig. 1b-c**). Gemcitabine monotherapy resulted in comparable tumour regression in both HRD and HRP xenografts (0.75 *vs.* 0.60, $p = 0.46$). Similarly, there was no difference in treatment response to combination gemcitabine-cisplatin or gemcitabine-talazoparib between HRD *vs.* HRP xenografts.

Cisplatin-talazoparib combination resulted in greater tumour inhibition compared to talazoparib alone in both HRD (1.46 *vs.* 2.35, p = 0.040) and HRP xenografts (4.19 *vs.* 5.73, p = 0.036). In HRD xenografts, there was a trend towards improved efficacy with cisplatin-talazoparib compared to cisplatin alone (1.46 *vs.* 2.50, p = 0.087); however, no difference was seen for HRP xenografts (4.19 *vs.* 4.97, p = 0.280).

3. Gemcitabine-cisplatin is associated with prolonged survival in HRD PDAC xenografts

Since HRD and HRP xenografts had similar tumour regression following 28 days of gemcitabine mono- or combination therapy, we assessed differences in treatment durability. We compared the median overall survival (mOS) of mice in each treatment arm (gemcitabine *vs.* gemcitabine-cisplatin *vs.* gemcitabine-talazoparib) for HRD and HRP xenografts. Since mice were monitored until their tumour reached endpoint size, we used mOS as a surrogate for treatment durability. In mice bearing HRD tumours, gemcitabine-cisplatin was associated with significantly longer mOS compared to gemcitabine alone (126 *vs.* 106.5 days, p = 0.048) and gemcitabine-talazoparib (126 *vs.* 98 days, p < 0.001). There were no differences in mOS between gemcitabine and gemcitabine-talazoparib (106.5 *vs.* 98 days, p = 0.14). Median overall survival was similar between all 3 treatment arms in HRP xenografts (**Fig. 1d-e**).

Gemcitabine-talazoparib was the most toxic regimen, with 31% of mice euthanized prior to the end of treatment. This contrasts with the 9% and 0% on-treatment mortality in the

gemcitabine-cisplatin and gemcitabine monotherapy arms, respectively. To adjust for regimen-related toxicity, we repeated the survival analyses including only mice that completed 28 days of treatment. In HRD tumours, gemcitabine-cisplatin was again associated with longer mOS compared to gemcitabine alone (130 *vs.* 106.5 days, p = 0.002) and gemcitabine-talazoparib (130 *vs.* 109 days, p = 0.020). Median OS was comparable between all 3 treatment arms for HRP tumours (**Supp. Fig. 2**).

4. Gemcitabine-cisplatin and gemcitabine-talazoparib suppress tumour proliferation in HRD xenografts

To investigate the antiproliferative effect of gemcitabine-based therapy, we evaluated the Ki67 index of PDXs at the end of treatment (day 29). HRD PDX treated with gemcitabine-cisplatin (0.34 *vs.* 0.57, p = 0.040) and gemcitabine-talazoparib (0.23 *vs.* 0.60, p < 0.001) had a significantly lower relative Ki67 index compared to HRP tumours (**Fig. 2a-b**). With gemcitabine monotherapy, HRD PDX also had a lower relative Ki67 index (0.38 *vs.* 0.63, p = 0.161), although this trend was not statistically significant. Additionally, the Ki67 index was significantly correlated with mitotic activity across all PDX (R = 0.692, p < 0.001) (**Fig. 2c**). Further, we evaluated cleaved caspase-3 (CC-3) immunostaining as a marker of apoptotic cell death. Gemcitabine-talazoparib was associated with significantly increased relative CC-3 positivity in HRD *vs.* HRP PDX (4.94 vs. 1.79, p = 0.006; **Supp. Fig. 3**). Four cases (3 HRD, 1 HRP) had minimal

residual tumour at the end of treatment, and were insufficient for Ki67 and CC-3 immunostaining.

5. Longitudinally-derived HRD xenografts recapitulate the emergence of clinical chemoresistance

To study the evolution of treatment response to HRD-targeted therapies, we longitudinally derived 3 xenografts from a patient with biallelic *BRCA2*-mutated PDAC, over a 4.5-year disease course (**Fig. 3a-b**). The patient presented with a pancreatic tail PDAC and liver metastases. Following an exceptional response to FOLFIRINOX, a distal pancreatectomy (PDX #1, Q70P) and radiofrequency ablation of his liver metastases were performed. Two years later, a second xenograft was established (PDX#2, Q70LM) from new liver metastases. These liver metastases again responded to FOLFIRINOX. Finally, a third xenograft (PDX #3, Q70AM) was established from an abdominal wall metastasis at the time of disease progression. The patient died after 2 additional cycles of platinum-based therapy (gemcitabine-cisplatin).

To represent each patient by a single PDX, only the Q70P xenograft was included in the preclinical trial summarized in Figure 2. However, we also performed the 7-arm preclinical trial for the 2 longitudinal PDXs (Q70LM, Q70AM) to evaluate their treatment sensitivities (117 mice in total). The Q70P and Q70LM xenografts showed sensitivity to

cisplatin (Q70P, 4.19 *vs.* 11.25 fold change, $p < 0.001$; Q70LM, 2.60 *vs.* 6.20, $p < 0.001$), talazoparib (Q70P, 2.26 *vs.* 11.25, $p < 0.001$; Q70LM, 1.52 *vs.* 6.20, $p < 0.001$) and cisplatin-talazoparib (Q70P, 1.56 *vs.* 11.25, $p < 0.001$; Q70LM, 1.15 *vs.* 6.20, $p < 0.001$) compared to vehicle, mirroring the clinically favourable response to FOLFIRINOX (**Fig. 3c**). In contrast, the Q70AM xenograft showed resistance to cisplatin (4.00 *vs.* 4.92, $p = 0.22$) and talazoparib (4.40 *vs.* 4.92, $p = 0.69$) monotherapy. However, this xenograft remained sensitive to cisplatin-talazoparib combination (2.29 *vs.* 4.92, $p < 0.001$).

To understand the mechanisms underlying this acquired resistance, we whole genome sequenced the patient's abdominal wall metastasis (Q70AM). The germline and somatic inactivating *BRCA2* mutations found in the Q70P tumour were conserved in the Q70AM tumour. Both tumours had elevated HRDetect scores (>0.99) and had SNV mutational patterns dominated by SBS3 (**Fig. 4a**). However, while the Q70P tumour was diploid, the Q70AM tumour was polyploid. The liver metastasis (Q70LM) sample had insufficient cellularity for WGS, but we determined that it had also become polyploid using SNP array profiling and flow cytometric cell cycle analysis (**Supp. Fig. 4**).

6. A genomic scar persists in HRD xenografts treated with gemcitabine-cisplatin

To characterize changes in the genomic landscape of HRD xenografts following 28 days of treatment, we whole genome sequenced 4 *BRCA2*-mutated PDAC trios. These

included (1) patient primary, (2) untreated parent PDX and (3) PDX treated with gemcitabine-cisplatin (GC) for 28 days, and collected at humane endpoint. We profiled xenografts from the GC arm, since this regimen showed the strongest and most sustained treatment response. We hypothesized that tumours that regrew following treatment cessation would have an increase in non-HRD-associated mutational signatures related to expansion of resistant subclonal populations under selective therapy pressure. Additionally, to evaluate the impact of prior chemotherapy exposure, we characterized PDXs from patients that were both chemo-naïve (Q392, O232) and chemo-treated (Q70P, Q70AM).

Germline and somatic *BRCA2* mutations were conserved in both the untreated parent and GC-treated xenografts across all trios, and there was no evidence of a reversion mutation in trial endpoint PDXs (**Fig. 4a**). Similarly, HRDetect scores remained high (>0.99) in both untreated parent and GC-treated xenografts. There was no significant decrease in SBS3 proportion in the GC-treated xenografts, compared to the untreated parent xenografts (26.3 *vs.* 29.3%, p = 0.89).

Next, we evaluated the SNVs private to the GC-treated xenografts, and which presumably accumulated on treatment. Interestingly, these private SNVs continued to show SBS3 mutational patterns (**Supp. Fig. 5)**. In 3 of 4 cases, we also observed SBS3 variants private to the untreated parent xenograft, suggesting that a fraction of HRD clones may have been eradicated with GC. Another important observation was that the

298 Q70AM tumour, which was chemoresistant both clinically and in the preclinical trial,
299 retained an elevated SBS3 proportion and HRDetect score. These data suggest that a
300 genomic HRD scar persists despite the emergence of resistance.
301
302 GC-treated xenografts had a higher neoantigen load compared to their matched
303 untreated xenograft (161 *vs.* 134, p = 0.02, **Fig. 4b**). Importantly, the Q70AM patient
304 tumour, which received several additional cycles of platinum-based chemotherapy
305 compared to the Q70P primary, exhibited a higher neoantigen load (122 *vs.* 82). This
306 observation was corroborated by a higher degree of CD8+ cytotoxic T-cell infiltration in
307 the Q70AM tumour compared to the Q70P primary, albeit not to levels typically seen in
308 mismatch repair-deficient PDAC (**Fig. 4c**).
309
310 *7. Tumour polyploidy and low Ki67 associated with poor response to platinum and*
311 *PARPi*
312
313 Among xenografts exhibiting genomic HRD hallmarks, we observed heterogeneity in
314 individual tumour responses to cisplatin and talazoparib therapy. We searched for
315 additional biomarkers that may be predictive of treatment response. All HRD and HRP
316 xenografts were whole transcriptome sequenced, and their Moffitt transcriptomic
317 subtype was determined relative to 167 PDAC transcriptomes, 164 of which were
318 sequenced in the COMPASS trial[23] (NCT02750657). Of the 8 HRD xenografts, 4 were
319 basal-like, whereas the remaining 4 were classical. All HRP xenografts were classical

(**Fig. 5a**). Additionally, all HRP xenografts were profiled using a SNP array to determine their ploidy (**Supp. Fig. 4**).

We performed stepwise multivariate linear regression to identify independent predictors of cisplatin (**Fig. 5b**) and talazoparib (**Fig. 5c**) response. In the cisplatin model, genomic hallmarks of HRD ($\beta = -0.478$, $p < 0.001$) and a higher Ki67 ($\beta = -0.257$, $p = 0.005$) were independently associated with better response, whereas tumour polyploidy ($\beta = 0.600$, $p < 0.001$) was associated with poor response. In the talazoparib model, HRD genomic hallmarks ($\beta = -0.299$, $p = 0.002$) and a basal-like transcriptomic subtype ($\beta = -0.442$, $p < 0.001$) were predictive of treatment response. A higher Ki67 index ($\beta = -0.192$, $p = 0.059$) was also associated with better talazoparib response, although this trend missed statistical significance. Tumour polyploidy ($\beta = 0.449$, $p < 0.001$) was again associated with poor response in the talazoparib model.

To illustrate the heterogeneity in treatment responses across individual xenografts, we performed principal component analysis (PCA) followed by k-means clustering to group xenografts based on their sensitivity to cisplatin, talazoparib and cisplatin-talazoparib (**Supp. Fig. 6**). Cluster 1 identified the best responders, of which all were HRD and diploid, except Q70LM which was a polyploid HRD case with high Ki67. Cluster 2 represented the intermediate responders, which included an HRP case (Q155), a case with monoallelic *BRCA2* inactivation and low HRDetect score (Q437) and a polyploid HRD case with high Ki67 (S145). Cluster 3 identified the xenografts with the worst

342 treatment response, of which 2 were HRP, while the third was a polyploid, low-Ki67,
343 HRD case that had developed chemoresistance (Q70AM).
344
345 Across the xenografts evaluated in the preclinical trial, we observed sustained complete
346 responses in 2 cases: O217 and O28. Interestingly, both were diploid, high Ki67, HRD
347 cases from Cluster 1. Both xenografts showed sustained complete responses with
348 gemcitabine-cisplatin (median follow-up 237 days) and cisplatin-talazoparib (median
349 follow-up 248 days). The O217 case also showed a sustained complete response with
350 gemcitabine-talazoparib (median follow-up 252 days).
351
352
353 *8. Tumour polyploidy and a basal-like transcriptomic subtype are associated with*
354 *worse prognosis in HRD PDAC*
355
356 To evaluate the prognostic relevance of these biomarkers, we identified 21 patients with
357 PDAC exhibiting genomic HRD hallmarks based on WGS. In addition to the 6 patients
358 whose tumours were evaluated in the preclinical trial, we also included 12 HRD PDAC
359 patients enrolled in the COMPASS trial and 3 additional HRD PDAC patients with whole
360 genome and whole transcriptome sequencing data (**Supp. Table 2**).
361
362 The median OS for all patients was 25.9 months (95% CI 0-51.9 months). Patients with
363 polyploid tumours had shorter mOS compared to those with diploid tumours (13.8 *vs.*

53.9 months, p = 0.008) (**Fig. 6a**). Additionally, patients with a basal-like PDAC had shorter mOS compared to those of classical transcriptomic subtype (25.9 *vs*. 38.5 months, p = 0.081) (**Fig. 6b**). We performed a multivariable Cox regression analysis with stepwise forward selection, including age, sex, stage, tumour ploidy and Moffitt transcriptomic subtype. Tumour polyploidy (HR 8.6, p = 0.007) and a basal-like transcriptomic subtype (HR 5.0, p = 0.033) were independently associated with mortality (**Fig. 6c**). After adjusting for stage and sex, a basal-like subtype remained independently predictive of poor survival, whereas tumour polyploidy trended towards significance (**Supp. Fig. 7**).

This clinical series included 3 patients who have been disease-free for over 5 years, of which 2 initially presented with locally advanced disease. Interestingly, all 3 long-term survivors had classical, diploid HRD PDAC.

9. GATA6:KRT17 ratio is an immunohistochemical discriminator of classical versus basal-like transcriptomic subtype

Since basal-like HRD PDAC was associated with worse prognosis, we searched for clinically practical biomarkers that could robustly predict transcriptomic subtype. Using the combined COMPASS and PDX cohorts, we compared the normalized gene expression levels (log2CPM) of GATA6, KRT17 and KRT81 between classical and

basal-like PDAC. GATA6 expression was significantly higher in classical tumours (p = 2.53e-17) whereas KRT17 and KRT81 expression were significantly higher in basal-like tumours (KRT17, p = 1.59e-4; KRT81, p = 5.12e-4, **Fig. 7a**). To validate these findings, we performed IHC staining on tissue microarrays of HRD PDAC xenografts with known Moffitt subtype. High GATA6 staining was predictive of the classical subtype with an area under the curve (AUC) of 0.902, whereas high KRT17 staining was predictive of the basal-like subtype with an AUC of 0.828. The combination of these 2 markers as a GATA6:KRT17 ratio had higher predictive value than either marker alone, with an AUC of 0.971 (**Fig. 7b-d**). Using a clinically pragmatic cutoff of 1, the GATA6:KRT17 ratio has a sensitivity of 100% and a specificity of 83.3%.

We also performed multiplex IHC (mIHC) to investigate the colocalization of these seemingly complementary markers. Tumours stained predominantly for one of the two markers, and only 14.9% of cells were dual-positive for GATA6 and KRT17. Interestingly, we observed discrete subpopulations of GATA6+/KRT17- and GATA6-/KRT17+ cells within the same xenograft (**Fig. 7e**). This intratumoral heterogeneity was also found in the corresponding patient tumour (**Supp. Fig. 8**). Finally, we found KRT81 IHC to be a poor predictor of transcriptomic subtype, with an AUC of 0.519.

10. Cell lines derived from polyploid HRD PDAC xenografts are spontaneously immortal

We established primary cell cultures from 8 g*BRCA*-mutated patient-derived xenografts (**Supp. Table 3**). Of these, 3 cell lines were spontaneously immortal, and could be propagated beyond 40 passages without exogenous growth factor stimulation. Interestingly, these immortal cell lines were all derived from polyploid tumours (Q70LM, Q70AM, S145). In contrast, the 5 remaining primary cell cultures that were generated from diploid PDAC xenografts could only be maintained *in vitro* for a finite period, becoming senescent within two passages.

Discussion

The advent of next-generation sequencing (NGS) has accelerated the identification of molecular subtypes of PDAC with targeted therapy opportunities. However, comparing molecular-guided treatments head-to-head using conventional clinical trial designs is impractical[24,25]. To overcome these challenges, we combined a multi-institutional patient cohort and rare PDX models to identify biomarkers underlying the therapeutic and prognostic heterogeneity of g*BRCA*-mutated PDAC, which is the most prevalent druggable PDAC subtype.

We found that biallelic, but not monoallelic, inactivation of *BRCA1*/*BRCA2* was associated with mutational signatures characteristic of HR deficiency, including SBS3 and HRDetect. We showed that xenografts exhibiting HRD genomic hallmarks were preferentially sensitive to cisplatin, talazoparib, and the combination of these therapies. This has important treatment and economic implications, considering that routine germline testing is becoming standard of care in PDAC[26], and there is indication to treat *gBRCA*-mutated platinum-sensitive PDAC with PARPi based on the POLO trial[17]. However, cases of monoallelic *BRCA1/BRCA2* inactivation may not respond to platinum and PARPi therapies. Therefore, integration of companion FFPE tissue-based NGS assays (Myriad myChoice HRD, FoundationFocus $CDx_{BRCALOH}$) will be important to improve selection of patients for therapies targeting HR deficiency[27,28].

Treatment responses to gemcitabine-cisplatin and gemcitabine-talazoparib were comparable between HRD *vs.* HRP xenografts, and were driven by the high efficacy of gemcitabine. Considering the clinical response rates to gemcitabine, these preclinical observations may reflect differences in intratumoral drug delivery and tumour immune microenvironment in subcutaneous xenograft models. Nonetheless, the combination of gemcitabine-cisplatin yielded the most durable treatment response in our preclinical trial, in addition to a significant antiproliferative effect compared to gemcitabine alone.

Akin to clinical observations[17], we found heterogeneity in treatment responses among the HRD PDAC xenografts. We identified tumour polyploidy as an independent predictor of poor platinum and PARPi response. This finding is consistent with previous reports showing that polyploid cells are resistant to cytotoxic drugs[29,30]. We also found that xenografts with a higher Ki67 index had a better response to cisplatin. We identified a similar trend with talazoparib, although this did not achieve statistical significance, possibly reflecting our sample size. These observations are in concordance with studies in triple-negative breast cancer and enteropancreatic neuroendocrine tumours, in which a high Ki67 index predicts better initial responses to chemotherapy, but do not translate to improved survival. To this end, Ki67 index did not correlate with survival in our study, and its prognostic value in HRD PDAC remains unclear.

Additionally, in our cohort of HRD PDAC patients, tumour polyploidy was independently predictive of shorter survival. Importantly, this biomarker can be readily integrated into

routine testing of clinical specimens using SNP genotyping assays that capture genome-wide copy number aberrations.

Interestingly, we found that cell lines derived from polyploid g*BRCA*-mutated tumours were spontaneously immortal, whereas those generated from diploid tumours became senescent. These observations support polyploidy as an aggressive tumour characteristic, and are consistent with our finding of polyploidy as a marker of poor treatment response and prognosis in g*BRCA*-mutated PDAC. Capan-1, the only published *BRCA2*-mutated pancreatic cancer cell line, has a hypotriploid genome[31]. We provide three additional polyploid g*BRCA*-mutated cell lines for *in vitro* studies. Importantly, the S145 cell line represents the first human *BRCA1*-mutated PDAC cell line.

Although the Q70AM xenograft was resistant to cisplatin and talazoparib monotherapies, combination of these therapies yielded a treatment response. We also observed an additive treatment benefit when combining cisplatin with talazoparib in the preclinical trial. These findings suggest a synergistic effect of combining platinums and PARPi in HRD PDAC. Importantly, talazoparib is a second-generation PARPi with higher PARP1 trapping potency and relatively high catalytic inhibition compared to earlier generation PARPis (e.g., olaparib and veliparib), which have been previously studied in PDAC. Our findings are the first to demonstrate the preclinical efficacy of

479 talazoparib in multiple patient-derived tumours, providing motivation to evaluate
480 talazoparib alone or in combination with platinums in a clinical trial setting.
481
482 This study is the first to investigate the implications of Moffitt transcriptomic subtypes in
483 HRD PDAC. We identified a similar proportion of classical *versus* basal-like PDAC in
484 our series compared to published cohorts[3,23]. The basal-like subtype has been
485 associated with shorter survival, and poor response to 5-FU/leucovorin (adjuvant)[32] and
486 FOLFIRINOX (metastatic first-line)[23] in PDAC. In our HRD PDAC series, we found that
487 a basal-like transcriptomic subtype was independently predictive of worse prognosis.
488 Since there is growing evidence that discriminating between basal-like and classical
489 transciptomic subtypes has clinical implications not only for HRD PDAC but across
490 PDAC, we developed a novel, clinically pragmatic two-marker immunohistochemical
491 assay (GATA6:KRT17). We showed its ability to discriminate between the classical and
492 basal-like subtypes with 100% and 83.3% sensitivity and specificity, respectively.
493
494 For advanced-stage g*BRCA*-mutated PDAC, retrospective series have shown a survival
495 benefit with platinum-based therapy[7,14,16]. In this preclinical trial, the Moffitt subtype was
496 not predictive of response to cisplatin after adjusting for HRD genomic hallmarks. This
497 findings suggests a hierarchy where HRD genomic features dictate platinum sensitivity
498 over transcriptomic subtype.
499

We found that xenografts treated with gemcitabine-cisplatin retained genomic hallmarks of HRD and an elevated HRDetect score. Similarly, we demonstrated in a longitudinal study that a patient tumour that had acquired clinical chemoresistance retained a high HRDetect score. These findings suggest that HRD tumours develop a genomic scar that is the result of HRD-driven genomic mutations, and that these genomic hallmarks may not be an accurate indicator of ongoing sensitivity to HRD-targeting therapies. Thus, integrating functional assays, such as the RAD51 assay, alongside mutational signature-based biomarkers, may be a more precise strategy to select patients likely to benefit from HRD-targeted therapy[33,34].

Comparison of untreated *vs.* GC-treated PDXs revealed SBS3 variants private to the untreated xenografts, suggesting that a fraction of HRD clones may have been eliminated with treatment. This observation provides support that therapies targeting HR deficiency can eradicate, rather than only suppress, HRD PDAC cells.

We have previously shown that HRD PDAC typically exhibits a higher mutational burden than “sporadic” PDAC, albeit lower than mismatch-repair deficient PDAC[35]. The inherent susceptibility of HRD PDAC to platinum-induced DNA damage may accelerate the production of tumour-specific neoantigens, and promote an antitumour immune response. In this study, we found an increase in neoantigen load in HRD PDAC xenografts following treatment with gemcitabine-cisplatin. This observation was corroborated by a longitudinal patient case treated with FOLFIRINOX, which revealed a

parallel increase in peritumoral cytotoxic T-cell infiltration that coincided with exposure to platinum-based treatment exposure. Thus, HRD PDAC may be well-suited to treatment approaches that strategically combine or sequence platinum-based therapies, or even PARPi, with immunotherapy[36,37].

In summary, we combined a multi-institutional patient cohort and rare preclinical models to develop a treatment sensitivity and prognostic model (**Fig. 8**) of g*BRCA*-mutated PDAC. Further, we introduce a novel, clinically pragmatic 2-marker assay that is predictive of transcriptomic subtype and suggest a potential role for platinum-PARPi combinations as well as immunotherapy approaches in HRD PDAC.

Materials and Methods

Patients

Patients with germline *BRCA1* or *BRCA2*-mutated PDAC were identified from 3 institutions: McGill University Health Centre, Montreal, Canada; Princess Margaret Cancer Centre, Canada; Chaim Sheba Medical Centre, Israel. Patients enrolled in the COMPASS molecular profiling trial (NCT02750657) from December 2015 to April 2019 were also included. Patient demographics, surgical procedure, chemotherapy treatment, and survival data were abstracted from prospectively maintained institutional research databases. Clinical staging was based on the 8th edition of the American Joint Committee on Cancer (AJCC) for pancreatic ductal adenocarcinoma. Survival was calculated from the initial date of pathologic diagnosis until death or censor date.

Germline sequencing of homologous recombination proficient cases

Homologous recombination proficient (HRP) cases included in the preclinical trial were identified by sequencing for germline mutations in HRD genes using a targeted panel of 710 cancer-related genes, including full gene sequencing of *BRCA1*, *BRCA2*, *PALB2* and *ATM*. The targeted regions were captured using Agilent SureSelect technology (Agilent Technologies, Santa Clara, CA, USA). Samples were sequenced on the

Illumina MiSeq platform (Illumina Inc., San Diego, CA, USA) with 300 base paired-end reads.

Whole genome sequencing (WGS)

Fresh frozen human and xenograft tumour tissue underwent laser capture microdissection for tumour cell enrichment prior to DNA extraction. WGS of tumour and matched lymphocyte DNA was performed at the Ontario Institute for Cancer Research using established institutional pipelines[38]. Germline and somatic variant calling, ploidy determination, neoantigen quantification protocols have been previously described. HRDetect scores were calculated as described by Davies et al[39]. Mutational signature proportions were derived by applying a non-negative least squares linear algorithm, as previously reported[40]. All germline mutations and somatic hits were confirmed in xenografts by Sanger sequencing.

RNA sequencing

Xenograft tumour tissues were preserved in RNAlater, and disrupted and homogenized using the Qiagen TissueLyser II (Qiagen, Manchester, UK). RNA was extracted using the Qiagen RNeasy Plus Universal Mini Kit (Qiagen, Manchester, UK). Sequencing was

579 performed by BGI Americas and the McGill University Genome Quebec Innovation
580 Centre (MUGQIC). Libraries were sequenced on the Illumina HiSeq 2000 (BGI) or
581 HiSeq 2500 (MUGQIC) platforms with TruSeq V3 reagents, to generate 100bp paired-
582 end reads at a sequencing depth of 50 million reads.
583
584 Adaptor sequences and low-quality score bases (Phred score < 30) were trimmed using
585 Trimmomatic[41]. The resulting reads were aligned to the human genome reference
586 sequence (GRCh38/hg38), using STAR[42]. To remove possible contaminated reads
587 originating from mouse in xenograft samples, reads were also aligned to the
588 GRCm38/mm10 mouse, and the Disambiguate algorithm (version 1.0)[43] was used to
589 assign reads to individual species based on the highest quality alignment of the read
590 pair (**Supp. Fig. 9**). Count data (originating from human reads) for each sample were
591 obtained using HTSeq[44]. For downstream analyses, we excluded lowly-expressed
592 genes with an average read count lower than 10 across all of the samples. Raw counts
593 were normalized using the TMM algorithm (i.e., weighted trimmed mean of M-values),
594 implemented in edgeR R package[45] (version 3.22.5). Using the voom function in the
595 limma R package[46] (version 3.36.5), the data were converted to log-counts per million.
596 The removeBatchEffect function from limma was used to correct for both batch effects.
597 Heatmaps were constructed using unsupervised hierarchical clustering (ward.D2
598 method). Transcriptomic classification into classical and basal-like subtypes was
599 performed as described by Moffitt et al[3].
600

Establishment of patient-derived xenografts

Mice were housed in a pathogen-free facility, on a 12-hour light-dark cycle, with ad lib access to water and sterile rodent chow. Fresh PDAC tissue was obtained from the operating theater or interventional radiology suite, minced into 1mm^3 pieces, and subcutaneously implanted into the flanks of 6-8-week-old female SCID beige mice (Charles River, Wilmington, MA, USA). Xenografts were grown to 1cm^3, harvested and serially passaged into new SCID beige mice. Tumours were cryopreserved in fetal bovine serum (FBS) with 10% dimethyl sulfoxide.

Multi-arm preclinical trial design

Fourth-passage patient-derived tumours were implanted into the right and left flanks of 6-8 week old female SCID beige mice. When the tumour volume reached 120mm^3, mice were randomized to one of seven treatment arms with the goal of treating 6-10 mice per arm. The treatment arms were: (1) Cisplatin (Enzo Life Sciences, Brockville, ON, Canada) 4mg/kg, once weekly, intraperitoneal; (2) Talazoparib (Abmole Biosciences, Hong Kong) 0.33mg/kg, 5 days on/2 days off, oral gavage; (3) Cisplatin-Talazoparib combination; (4) Gemcitabine (LC Laboratories, Woburn, MA, USA) 100mg/kg, twice weekly, intraperitoneal; (5) Gemcitabine-Cisplatin combination; (6) Gemcitabine-

623 Talazoparib combination; (7) Vehicle (PBS) 5 days on/2 days off oral gavage, and once
624 weekly intraperitoneal. Since pilot experiments showed increased toxicity with
625 talazoparib (data not shown), we randomized at least 10 mice into the talazoparib arms,
626 in anticipation that a greater fraction of mice in these arms may not complete the
627 treatment course. Treatment was administered for 28 days, with half-dosing or skipped
628 dosing, if mice lost >10% or >12.5% of their original weight, respectively. Mice were
629 weighed, and tumours were measured by caliper twice weekly. Mice were euthanized
630 when the tumour volume exceeded $2cm^3$, or if they lost >20% of their original weight.
631
632
633 *Tissue Microarrays*
634
635 Tissue microarrays were constructed using an automated tissue microarrayer (TMA
636 Grand Master, 3DHistech, Budapest, Hungary). Freshly harvested PDX tumours were
637 fixed in 10% buffered formalin for 24 hours, and paraffin-embedded. Tumour cores
638 (2mm diameter) were punched from each donor paraffin-embedded block based on
639 previously demarcated areas on a corresponding H&E stained slide. Each individual
640 patient was represented by 2-3 unique PDX cores originating from early-passage mice.
641 Overall, 33 cores representing 12 unique HRD PDAC xenografts were prepared on a
642 TMA, which was sectioned at 4um thickness for subsequent immunohistochemical
643 analyses.
644

Single-marker and multiplex immunostaining

4um serial sections of tissue microarray and patient tumour blocks were cut for hematoxylin and eosin (H&E) staining and immunohistochemical (IHC) analyses. IHC was performed using the Discovery Ultra autostaining platform (Ventana Medical Systems, Tucson, AZ, USA). Slides were incubated with a primary antibody, followed by the corresponding horseradish peroxidase (HRP)-conjugated secondary antibody (OmniMap anti-mouse #760-4310 or OmniMap anti-rabbit #760-4311, Ventana), developed with 3,3'-diaminobenzidine (DAB) and counterstained with hematoxylin. Primary antibodies used were as follows: anti-Ki67 (30-9, Ventana, undiluted), anti-cleaved caspase-3 (Asp175, Cell Signaling Technology, 1:100), anti-CD8 (SP57, Ventana, undiluted), anti-pancytokeratin (AE1/AE3/PCK26, Ventana, undiluted), anti-GATA6 (D61E4, Cell Signaling Technology, 1:500), anti-KRT17 (17516-1-AP, Proteintech, 1:100), anti-KRT81 (11342-1-AP, Proteintech, 1:50). Multiplex chromogenic IHC was also performed on the Discovery Ultra platform, using chromogenic detection kits from Ventana (#750-124, DAB; #760-247, teal).

Image analyses

Immunostained slides were scanned using the Aperio Scanscope (Aperio Technologies, Vista, CA, USA) at 20x magnification. For Ki67 immunostaining, five regions of interest were randomly selected for each tumour, and manually annotated to exclude stromal and necrotic areas by a technician blinded to treatment assignment. Ki67 immunostaining was quantified by digital analysis of positively staining nuclei using the Aperio ImageScope software (Aperio Technologies, Vista, CA, USA). Cleaved caspase-3, GATA6, KRT17 and KRT81 immunostaining were quantified using the Halo (Indica Labs, Corales, NM, USA) cytonuclear algorithm (single-marker) or multiplex IHC algorithm (multiplex IHC). A tissue classifier was developed to automatically segment tumour from stroma and necrosis. Cell recognition and nuclear segmentation were optimized, and quality control was performed for each case.

Hematoxylin-eosin stained sections were reviewed by a board-certified gastrointestinal pathologist (S.F.). Mitotic figures were counted manually, and expressed as the number of mitotic figures per 10 high-power fields.

Generation of primary cell cultures from HRD xenografts

Harvested xenograft tumours were mechanically minced, and underwent serial trypsin digestion at 37°C. Murine fibroblast contamination was eliminated by magnetic-activated cell sorting using the Miltenyi Mouse Cell Depletion kit[47] (Miltenyi Biotec, Auburn, CA,

USA). Cells were seeded on collagen-coated plates and cultured in RPMI supplemented with 10% FBS and 1% antibiotic/antimycotic solution, at 37°C in a humidified incubator with a 5% CO_2 atmosphere. Cell numbers were counted by trypan blue exclusion assay with a hematocytometer at 24-hour intervals for 7 days. Cell doubling times were calculated using a nonlinear regression (exponential growth equation) analysis.

Tumour ploidy determination

Q70P, Q70LM and Q70AM primary cell lines were generated as described above. Cells were harvested by centrifugation, fixed with ethanol, and incubated in 0.5mL cell cycle buffer containing 30ug/mL propidium iodide (PI, Sigma-Aldrich, USA) and 50ug/mL RNase A (Thermo Scientific, USA). PI fluorescence data were collected from 10,000 cells on a flow cytometer, after gating to exclude dead cells, debris and doublets[48]. The Q70P cell line was used as a control to fix the voltage for the diploid population. DNA histograms were plotted using FlowJo (Tree Star Inc., Ashland, OR, USA).

To determine the ploidy of the HRP cases, genomic DNA was extracted from early-passage xenografts and single nucleotide polymorphism (SNP) array was performed using the Illumina Infinium Omni2.5 microarray. The allele-specific copy number analysis of tumors (ASCAT, v2.4.3) algorithm was used to infer tumour ploidy and tumour purity, as previously described[49]. Each sample was run independently in

710 “tumour-only” mode, using the 'Illumina2.5M' profile within ASCAT. The ploidy estimates
711 were compared across passages for each tumour.
712
713 *Statistics*
714
715 Statistical analyses were performed using R software version 3.5 (R Foundation for
716 Statistical Computing, Vienna, Austria) and Graphpad Prism, version 6 (Graphpad, CA,
717 USA). Differences between continuous variables were compared using the Wilcoxon
718 rank sum test. For forward stepwise multiple linear regression analysis, the criteria for
719 entry into the model was $p < 0.1$ and for removal was $p > 0.15$. Overall survival was
720 estimated using the Kaplan-Meier method and compared between treatment groups
721 using a log-rank test. Hazard ratios were calculated using the Cox proportional hazards
722 model. A p-value < 0.05 was considered statistically significant.
723
724 *Study Approval*
725 Use of human biospecimens and data was approved by the local institutional review
726 boards of each participating centre. Patients provided written informed consent to
727 participate. Animal studies were approved by the McGill University Animal Care
728 Committee, and conducted in accordance with Animal Research: Reporting of *In Vivo*
729 Experiments (ARRIVE) guidelines.

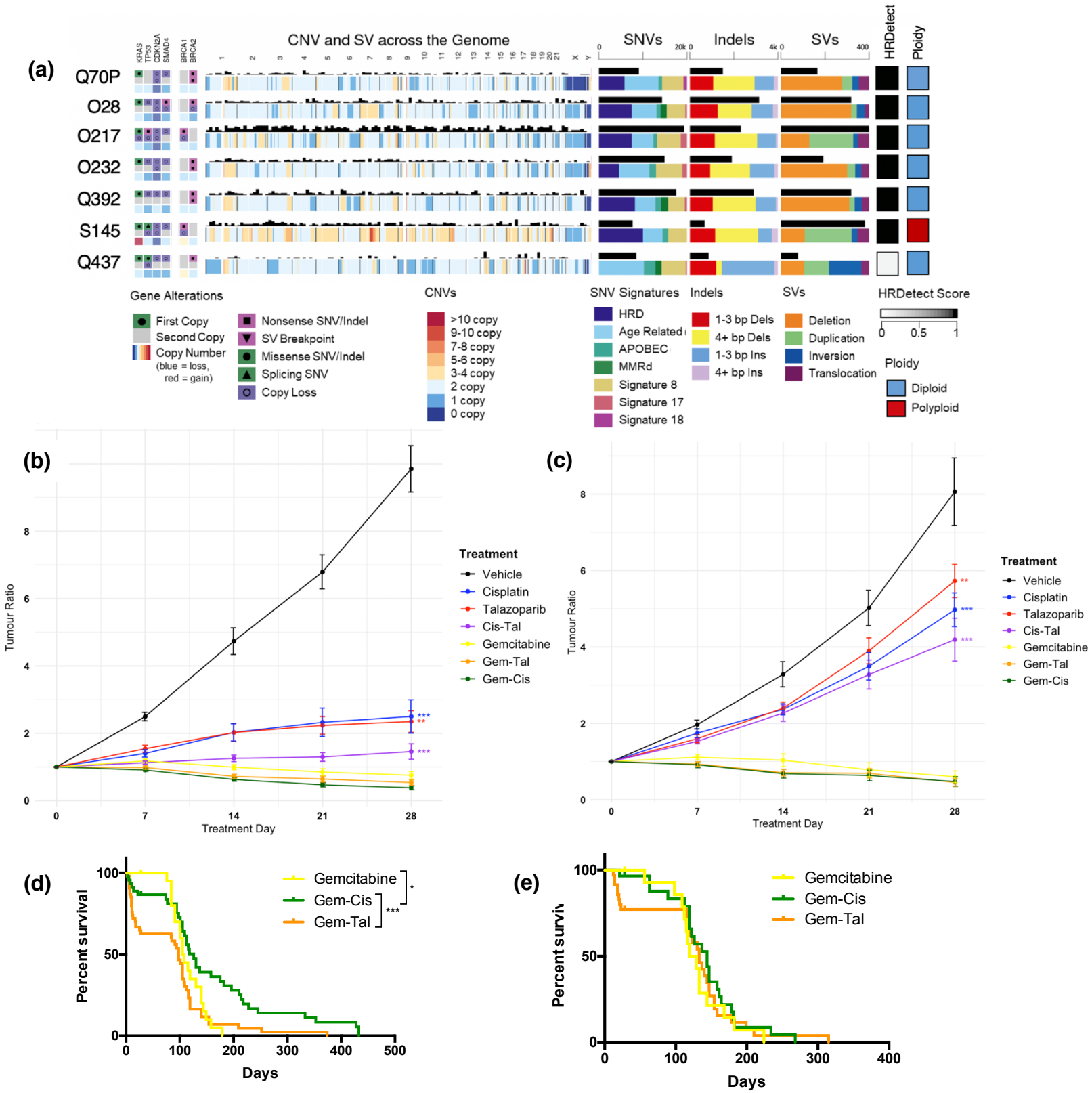

Figure 1. Genomic characteristics of patient-derived xenografts and preclinical trial outcomes. (a) Genomic characteristics of the 7 g*BRCA*-mutated PDAC cases evaluated in the preclinical trial. The first 6 cases have biallelic inactivation of *BRCA1* or *BRCA2*. They exhibit mutational patterns that are characteristic of homologous repair deficiency, and have an elevated HRDetect score. In contrast, the Q437 case with monoallelic *BRCA2* inactivation lacks these genomic HRD hallmarks and has a low HRDetect score. **(b-c)** 7-arm preclinical trial to evaluate response of PDAC xenografts to cisplatin, talazoparib and gemcitabine mono- and combination therapies. **(b)** HR-deficient (6 unique cases, 228 mice) and **(c)** HR-proficient (B, 4 unique cases, 159 mice) PDAC xenografts were treated for 28 days. For each treatment arm, the relative tumour growth (at Day 28) of HR-deficient *vs.* HR-proficient xenografts was compared using multiple linear regression models. Tal, talazoparib; ** $p < 0.01$; *** $p < 0.001$. **(d-e)** Kaplan-Meier survival curves of xenografts treated with gemcitabine mono- and combination therapies. In HR-deficient xenografts, gemcitabine-cisplatin was associated with longer survival than gemcitabine alone and gemcitabine-talazoparib. There was no survival difference in HR-proficient xenografts. P-values represent log-rank comparisons of Kaplan-Meier survival curves. * $p < 0.05$, ** $p < 0.01$, ** $p < 0.001$. Cis, cisplatin; Tal, talazoparib.

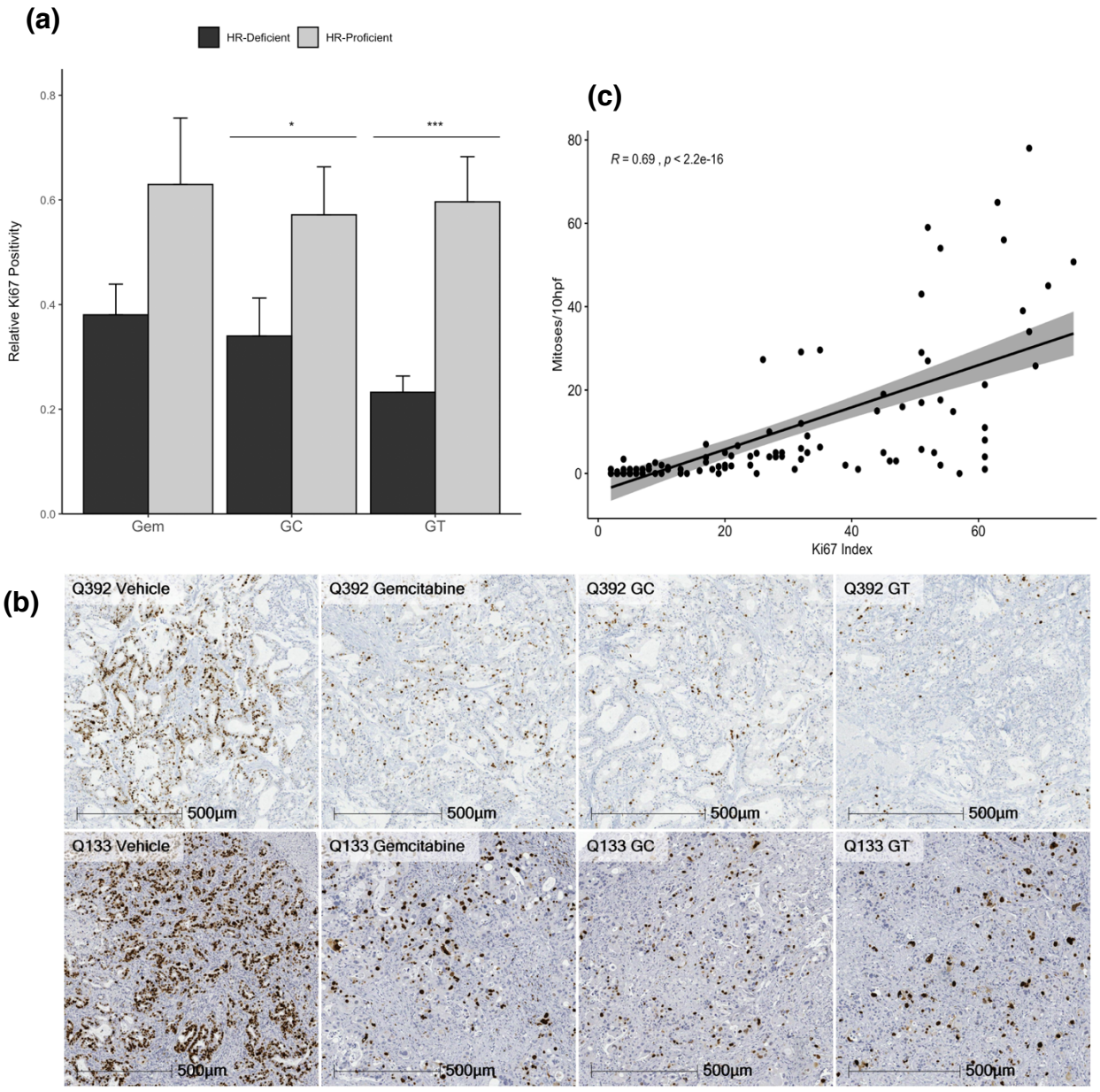

Figure 2. Histopathological and immunohistochemical analyses of proliferative activity in xenografts treated with gemcitabine mono- and combination therapies. **(a)** Comparison of relative Ki67 positivity of HR-deficient vs. HR-proficient xenografts for each treatment arm. * $p < 0.05$, *** $p < 0.001$. **(b)** Representative Ki67 immunostaining of Q392 (HR-deficient) *vs.* Q133 (HR-proficient) xenografts. GC, gemcitabine-cisplatin; GT, gemcitabine-talazoparib. **(c)** Pearson's correlation between absolute Ki67 positivity and mitotic activity (# mitoses/10hpf) across all xenografts.

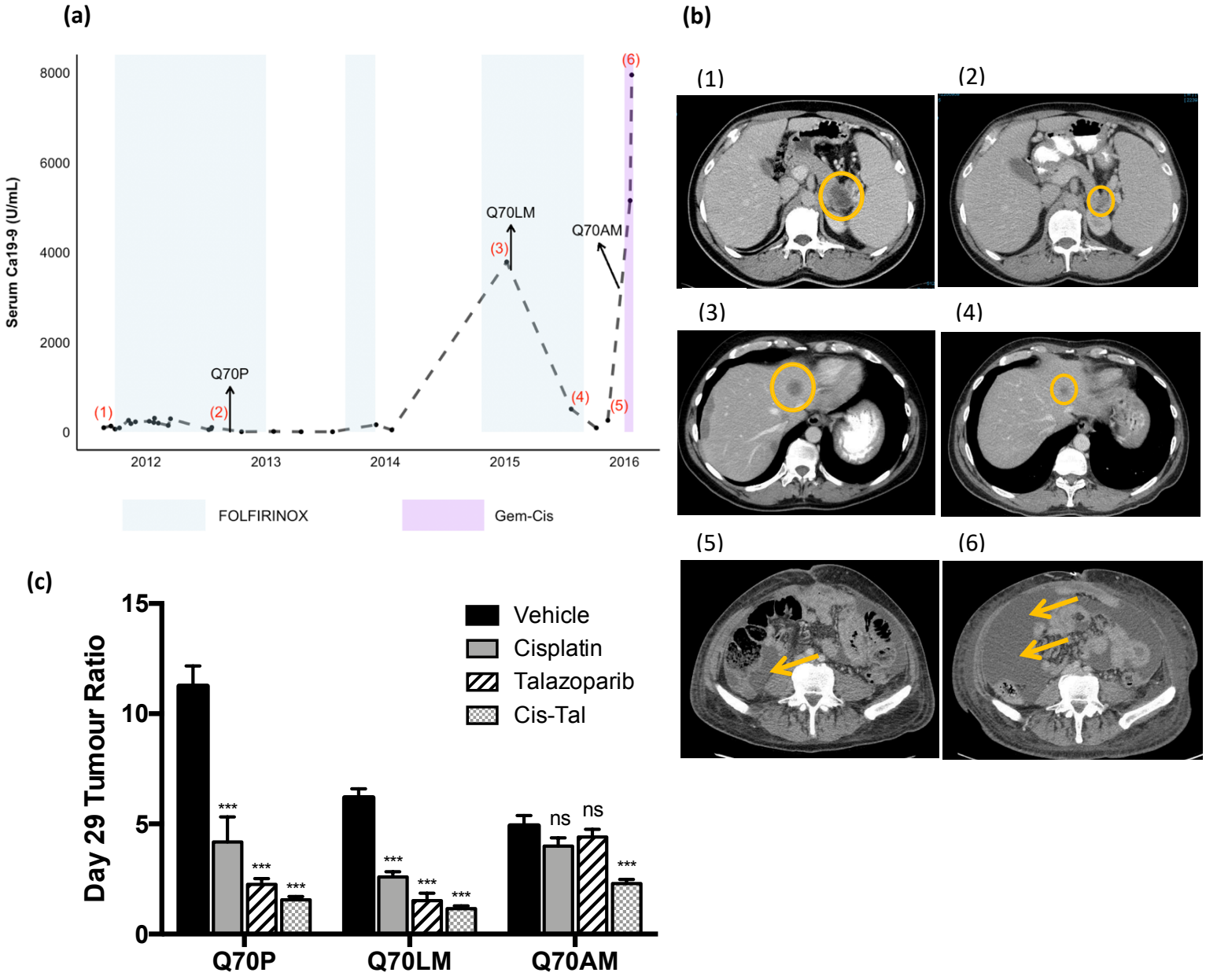

Figure 3. Longitudinally derived xenografts from a patient with HRD PDAC (Q70) recapitulate the emergence of clinical chemoresistance. (a) Timeline showing the evolution of serum Ca19-9 in relation to chemotherapy. Arrows indicate when the individual xenografts (Q70P, Q70LM, Q70AM) were derived. Numbers correspond to cross-sectional imaging detailed in (B). **(b)** Representative computed tomography scans showing chemotherapy response at various time points. **(1-2)** Partial response of the pancreatic tail primary (Q70P) to FOLFIRINOX. **(3-4)** Partial response of the liver metastases (Q70LM) to FOLFIRINOX. **(5-6)** Worsening of peritoneal carcinomatosis (Q70AM) on gemcitabine-cisplatin. **(c)** Multi-arm preclinical trial results for the Q70P, Q70LM and Q70AM xenografts (n = 117 mice). For a given xenograft, day 29 tumour ratios were compared between each treatment arm (cisplatin, talazoparib, cisplatin-talazoparib) and vehicle. The Q70AM xenograft showed resistance to cisplatin and talazoparib alone, but remained sensitivity to cisplatin-talazoparib combination. *** $p < 0.001$; ns, not significant. Tal, talazoparib.

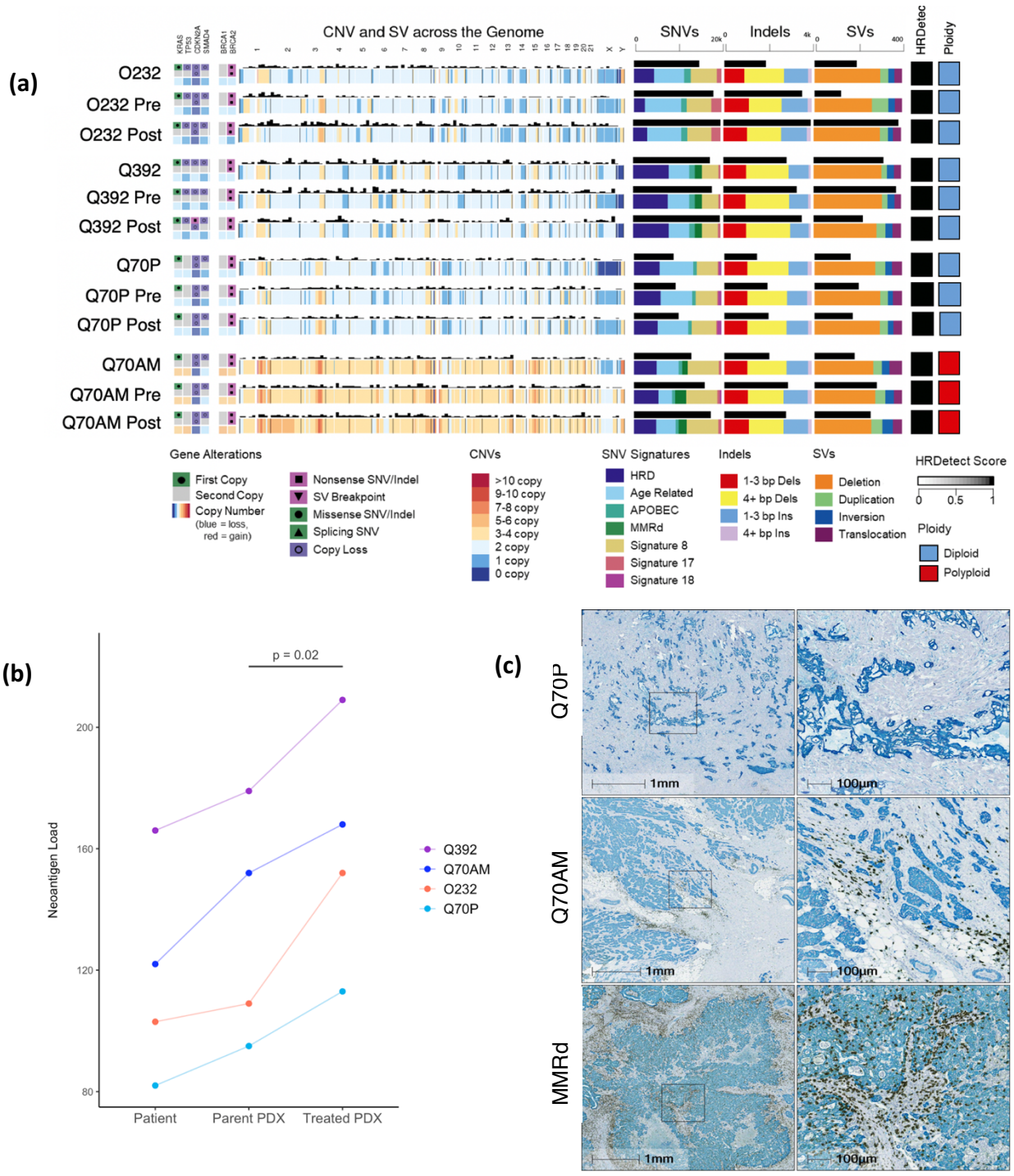

Figure 4. Whole genome sequencing (WGS) of 4 matched HRD PDAC trios to evaluate genomic changes on chemotherapy. (a) For each case, WGS of the (1) patient primary, (2) untreated parent PDX (Pre), and (3) PDX treated with gemcitabine-cisplatin and collected at trial endpoint (Post) are shown. Germline and somatic *BRCA2* mutations were conserved in all cases. The proportion of SBS3 remained stable in the gemcitabine-cisplatin-treated xenografts. **(b)** Evolution of neoantigen load between the patient, untreated parent PDX and PDX treated with gemcitabine-cisplatin. **(c)** Multiplex IHC stains showing spatial distribution of CD8+ (brown) cytotoxic T cells and pan-cytokeratin+ (teal) PDAC cells. Consistent with the increase in *in silico*-predicted neoantigens, there is an increase in CD8+ infiltration in the Q70AM tumour compared to the Q70P. However, the CD8+ infiltration remained less extensive compared to an MMR-deficient PDAC (MMRd).

(a)

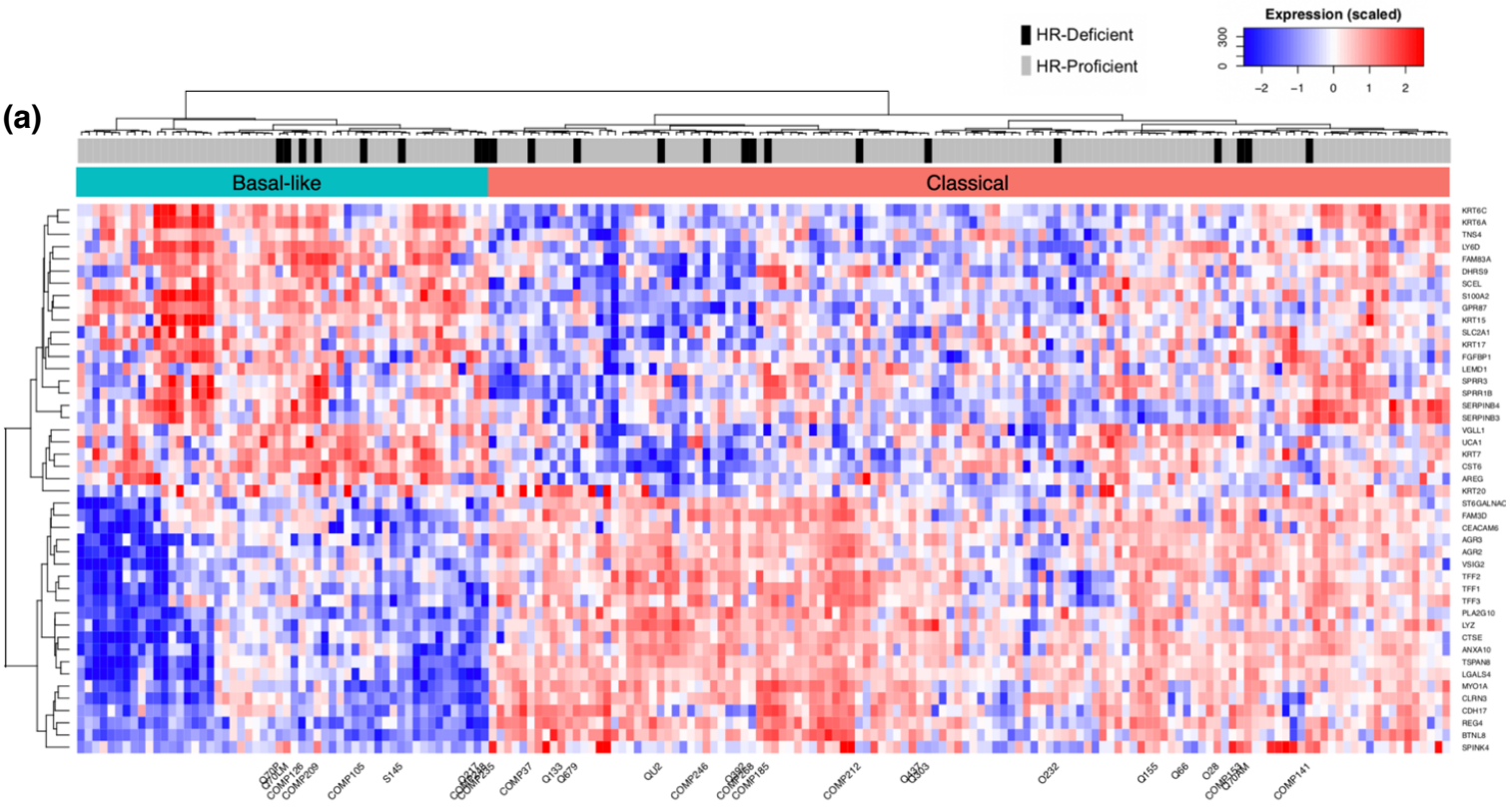

(b)

Variable	Standardized coefficient (β)	p-value
HRD	-0.478	<0.001
Ki67	-0.257	0.005
Polyploidy	0.600	<0.001

R^2 = 0.578
Excluded: Moffitt subtype, chemotherapy status

(c)

Variable	Standardized coefficient (β)	p-value
HRD	-0.299	0.002
Moffitt basal-like	-0.442	<0.001
Polyploidy	0.449	<0.001

R^2 = 0.780
Excluded: Ki67, chemotherapy status

Figure 5. Predictive biomarkers identified based on preclinical trial treatment responses. (a) Consensus clustered heatmap of PDAC transcriptomes split by Moffitt classical and basal-like factor gene expression. The 12 xenografts evaluated in the preclinical trial are identified, and clustered relative to 167 patient PDAC transcriptomes from the COMPASS trial (n = 164) and non-COMPASS patients (n = 3). The 21 HRD PDAC patients are indicated in black boxes. **(b)** Stepwise multivariable linear regression model of predictors of cisplatin response. **(c)** Stepwise multivariable linear regression model of predictors of talazoparib response

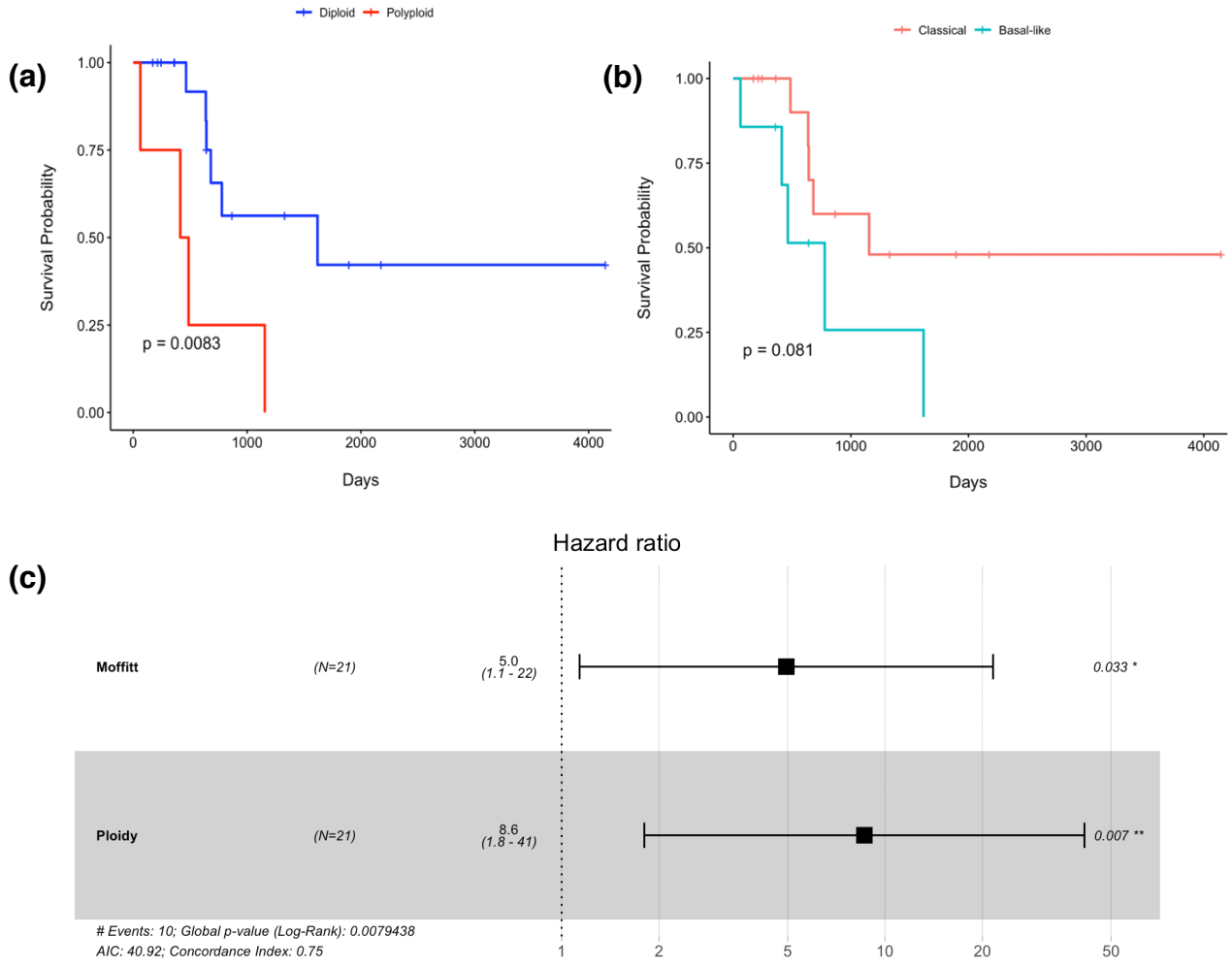

Figure 6. 21 Clinical outcomes of 21 HRD PDAC patients with whole genome and whole transcriptomic sequencing. Kaplan-Meier survival curves are shown, stratified by tumour ploidy **(a)** and transcriptomic subtype **(b)**. P-values represent log-rank comparisons. **(c)** Multivariable Cox regression analysis with forward stepwise selection, including age, sex, stage at diagnosis, tumour ploidy and Moffitt transcriptomic subtype. Tumour ploidy and Moffitt subtype were retained in the model and independently associated with survival. Hazard ratios and 95% confidence intervals are shown.

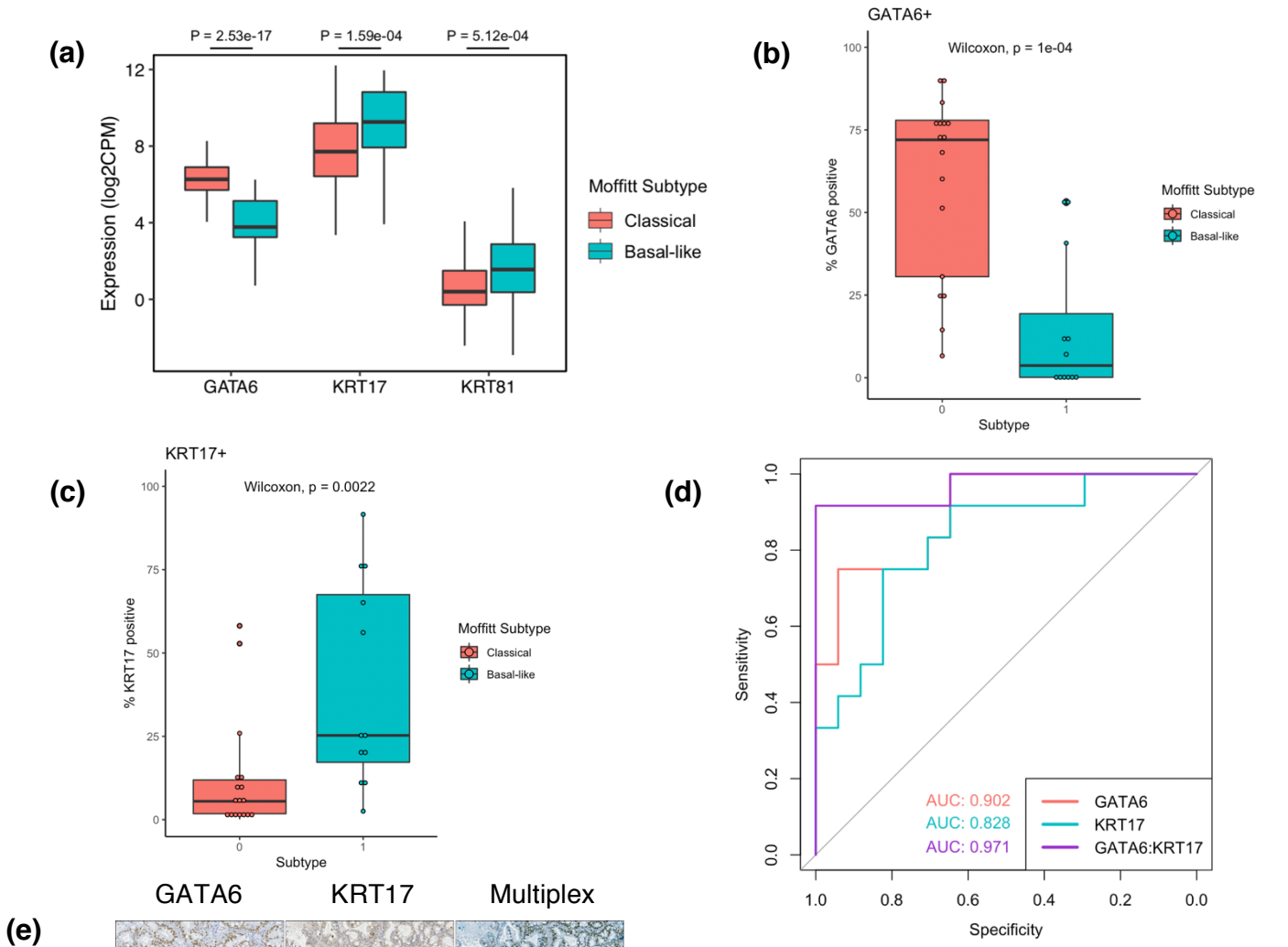

Figure 7. Immunohistochemical biomarkers of Moffitt transcriptomic subtype in HRD PDAC. **(a)** TMM-normalized log2(CPM) gene expression values for GATA6, KRT17 and KRT81 between classical and basal-like subtypes in the cohort described in Fig. 7. GATA6 and KRT17 were the most significantly correlated with transcriptomic subtype, and were further evaluated with IHC. **(b)** Classical HRD PDAC was associated with significantly higher GATA6 positivity. GATA6 immunostaining was quantified by digital image analysis using a tumor classifier and a nuclear scoring algorithm. **(c)** Basal-like HRD PDAC was associated with significantly higher KRT17 positivity, as assessed using a cytoplasmic scoring algorithm. **(d)** Combining both GATA6 and KRT17 as a GATA6:KRT17 ratio has higher predictive value than either marker alone. **(e)** Representative multiplex IHC stains showing GATA6 (brown) and KRT17 (teal). (Top row) Classical xenograft (O28) with predominantly GATA6+/KRT17- cells. (Middle row) Basal-like xenograft (S145) with predominantly GATA6-/KRT17+ cells. (Bottom row) Basal-like xenograft (Q70P) with a mutually exclusive mixture of GATA6-/KRT17+ cells and GATA6+/KRT17- cells, suggesting intratumoral heterogeneity.

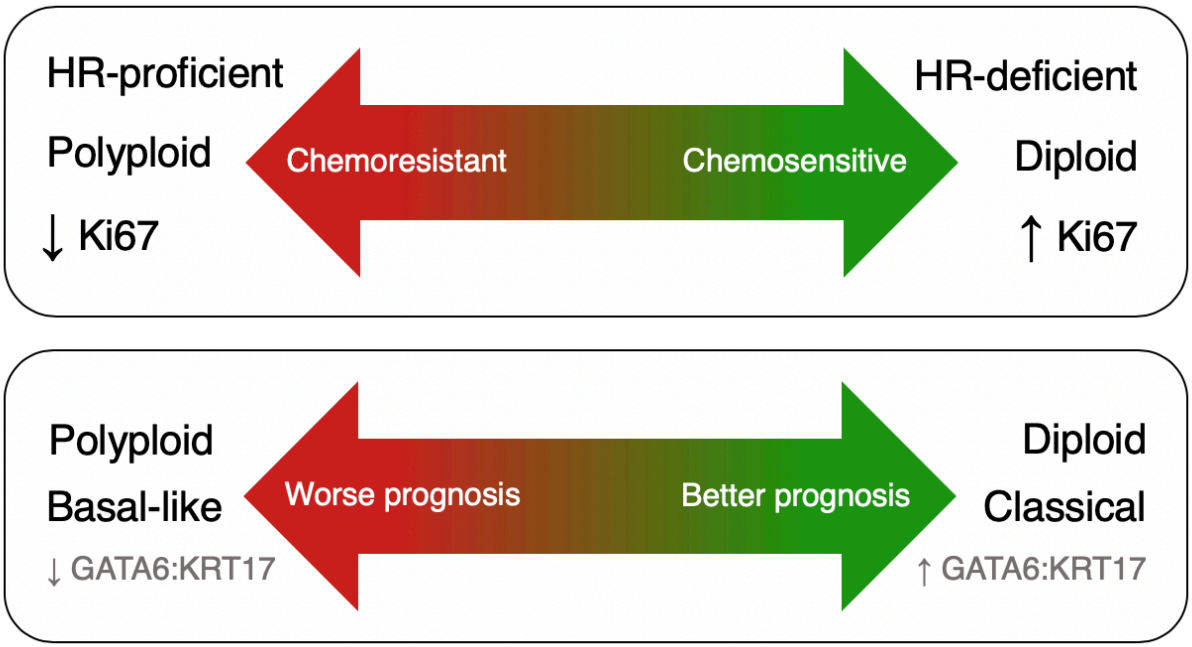

Figure 8. Proposed schematic of predictors of chemosensitivity and prognosis in HRD PDAC.

Figure Legends

Figure 1. Genomic characteristics of patient-derived xenografts and preclinical trial outcomes. (a) Genomic characteristics of the 7 g*BRCA*-mutated PDAC cases evaluated in the preclinical trial. The first 6 cases have biallelic inactivation of *BRCA1* or *BRCA2*. They exhibit mutational patterns that are characteristic of homologous repair deficiency, and have an elevated HRDetect score. In contrast, the Q437 case with monoallelic *BRCA2* inactivation lacks these genomic HRD hallmarks and has a low HRDetect score. **(b-c)** 7-arm preclinical trial to evaluate response of PDAC xenografts to cisplatin, talazoparib and gemcitabine mono- and combination therapies. **(b)** HR-deficient (6 unique cases, 228 mice) and **(c)** HR-proficient (B, 4 unique cases, 159 mice) PDAC xenografts were treated for 28 days. For each treatment arm, the relative tumour growth (at Day 28) of HR-deficient *vs.* HR-proficient xenografts was compared using multiple linear regression models. Tal, talazoparib; ** $p < 0.01$; *** $p < 0.001$. **(d-e)** Kaplan-Meier survival curves of xenografts treated with gemcitabine mono- and combination therapies. In HR-deficient xenografts, gemcitabine-cisplatin was associated with longer survival than gemcitabine alone and gemcitabine-talazoparib. There was no survival difference in HR-proficient xenografts. P-values represent log-rank comparisons of Kaplan-Meier survival curves. * $p < 0.05$, ** $p < 0.01$, ** $p < 0.001$. Cis, cisplatin; Tal, talazoparib.

Figure 2. Histopathological and immunohistochemical analyses of proliferative activity in xenografts treated with gemcitabine mono- and combination therapies. (a) Comparison of relative Ki67 positivity of HR-deficient vs. HR-proficient xenografts for each treatment arm. * $p < 0.05$, *** $p < 0.001$. **(b)** Representative Ki67 immunostaining of Q392 (HR-deficient) *vs.* Q133 (HR-proficient) xenografts. GC, gemcitabine-cisplatin; GT, gemcitabine-talazoparib. **(c)** Pearson's correlation between absolute Ki67 positivity and mitotic activity (# mitoses/10hpf) across all xenografts.

Figure 3. Longitudinally derived xenografts from a patient with HRD PDAC (Q70) recapitulate the emergence of clinical chemoresistance. (a) Timeline showing the evolution of serum Ca19-9 in relation to chemotherapy. Arrows indicate when the individual xenografts (Q70P, Q70LM, Q70AM) were derived. Numbers correspond to cross-sectional imaging detailed in (B). **(b)** Representative computed tomography scans showing chemotherapy response at various time points. **(1-2)** Partial response of the pancreatic tail primary (Q70P) to FOLFIRINOX. **(3-4)** Partial response of the liver metastases (Q70LM) to FOLFIRINOX. **(5-6)** Worsening of peritoneal carcinomatosis (Q70AM) on gemcitabine-cisplatin. **(c)** Multi-arm preclinical trial results for the Q70P, Q70LM and Q70AM xenografts (n = 117 mice). For a given xenograft, day 29 tumour ratios were compared between each treatment arm (cisplatin, talazoparib, cisplatin-talazoparib) and vehicle. The Q70AM xenograft showed resistance to cisplatin and talazoparib alone, but remained sensitivity to cisplatin-talazoparib combination. *** $p < 0.001$; ns, not significant. Tal, talazoparib.

Figure 4. Whole genome sequencing (WGS) of 4 matched HRD PDAC trios to evaluate genomic changes on chemotherapy. (a) For each case, WGS of the (1)

patient primary, (2) untreated parent PDX (Pre), and (3) PDX treated with gemcitabine-cisplatin and collected at trial endpoint (Post) are shown. Germline and somatic *BRCA2* mutations were conserved in all cases. The proportion of SBS3 remained stable in the gemcitabine-cisplatin-treated xenografts. **(b)** Evolution of neoantigen load between the patient, untreated parent PDX and PDX treated with gemcitabine-cisplatin. **(c)** Multiplex IHC stains showing spatial distribution of CD8+ (brown) cytotoxic T cells and pan-cytokeratin+ (teal) PDAC cells. Consistent with the increase in *in silico*-predicted neoantigens, there is an increase in CD8+ infiltration in the Q70AM tumour compared to the Q70P. However, the CD8+ infiltration remained less extensive compared to an MMR-deficient PDAC (MMRd).

Figure 5. Predictive biomarkers identified based on preclinical trial treatment responses. **(a)** Consensus clustered heatmap of PDAC transcriptomes split by Moffitt classical and basal-like factor gene expression. The 12 xenografts evaluated in the preclinical trial are identified, and clustered relative to 167 patient PDAC transcriptomes from the COMPASS trial (n = 164) and non-COMPASS patients (n = 3). The 21 HRD PDAC patients are indicated in black boxes. **(b)** Stepwise multivariable linear regression model of predictors of cisplatin response. **(c)** Stepwise multivariable linear regression model of predictors of talazoparib response.

Figure 6. 21 Clinical outcomes of 21 HRD PDAC patients with whole genome and whole transcriptomic sequencing. Kaplan-Meier survival curves are shown, stratified by tumour ploidy **(a)** and transcriptomic subtype **(b)**. P-values represent log-rank comparisons. **(c)** Multivariable Cox regression analysis with forward stepwise selection, including age, sex, stage at diagnosis, tumour ploidy and Moffitt transcriptomic subtype. Tumour ploidy and Moffitt subtype were retained in the model and independently associated with survival. Hazard ratios and 95% confidence intervals are shown.

Figure 7. Immunohistochemical biomarkers of Moffitt transcriptomic subtype in HRD PDAC. (a) TMM-normalized log2(CPM) gene expression values for GATA6, KRT17 and KRT81 between classical and basal-like subtypes in the cohort described in Fig. 7. GATA6 and KRT17 were the most significantly correlated with transcriptomic subtype, and were further evaluated with IHC. **(b)** Classical HRD PDAC was associated with significantly higher GATA6 positivity. GATA6 immunostaining was quantified by digital image analysis using a tumor classifier and a nuclear scoring algorithm. **(c)** Basal-like HRD PDAC was associated with significantly higher KRT17 positivity, as assessed using a cytoplasmic scoring algorithm. **(d)** Combining both GATA6 and KRT17 as a GATA6:KRT17 ratio has higher predictive value than either marker alone. **(e)** Representative multiplex IHC stains showing GATA6 (brown) and KRT17 (teal). (Top row) Classical xenograft (O28) with predominantly GATA6+/KRT17- cells. (Middle row) Basal-like xenograft (S145) with predominantly GATA6-/KRT17+ cells. (Bottom row) Basal-like xenograft (Q70P) with a mutually exclusive mixture of GATA6-/KRT17+ cells and GATA6+/KRT17- cells, suggesting intratumoral heterogeneity.

Figure 8. Proposed schematic of predictors of chemosensitivity and prognosis in HRD PDAC.

References

1. Siegel RL, Miller KD, Jemal A. Cancer statistics, 2019. *CA: A Cancer Journal for Clinicians*. 2019;69(1):7-34. doi:10.3322/caac.21551.

2. Rawla P, Thandra KC, Sunkara T. Pancreatic cancer and obesity: epidemiology, mechanism, and preventive strategies. *Clin J Gastroenterol*. 2019;12(4):285-291. doi:10.1007/s12328-019-00953-3.

3. Moffitt RA, Marayati R, Flate EL, et al. Virtual microdissection identifies distinct tumor- and stroma-specific subtypes of pancreatic ductal adenocarcinoma. *Nat Genet*. 2015;47(10):1168-1178.

4. Bailey P, Chang DK, Nones K, et al. Genomic analyses identify molecular subtypes of pancreatic cancer. *Nature*. 2016;531(7592):47-52. doi:10.1038/nature16965.

5. Collisson EA, Sadanandam A, Olson P, et al. Subtypes of pancreatic ductal adenocarcinoma and their differing responses to therapy. *Nat Med*. 2011;17(4):500-503. doi:10.1038/nm.2344.

6. Waddell N, Pajic M, Patch A-M, et al. Whole genomes redefine the mutational landscape of pancreatic cancer. *Nature*. 2015;518(7540):495-501. doi:10.1038/nature14169.

7. Smith AL, Wong C, Cuggia A, et al. Reflex Testing for Germline BRCA1, BRCA2, PALB2, and ATMMutations in Pancreatic Cancer: Mutation Prevalence and Clinical Outcomes From Two Canadian Research Registries. *JCO Precision Oncology*. 2018;(2):1-16. doi:10.1200/PO.17.00098.

8. Holter S, Borgida A, Dodd A, et al. Germline BRCA Mutations in a Large Clinic-Based Cohort of Patients With Pancreatic Adenocarcinoma. *J Clin Oncol*. 2015;33(28):3124-3129. doi:10.1200/JCO.2014.59.7401.

9. Chen C-C, Feng W, Lim PX, Kass EM, Jasin M. Homology-Directed Repair and the Role of BRCA1, BRCA2, and Related Proteins in Genome Integrity and Cancer. *Annu Rev Cancer Biol*. 2018;2(1):313-336. doi:10.1146/annurev-cancerbio-030617-050502.

10. Andrei A-Z, Hall A, Smith AL, et al. Increased in vitro and in vivo sensitivity of BRCA2-associated pancreatic cancer to the poly(ADP-ribose) polymerase-1/2 inhibitor BMN 673. *Cancer Lett*. 2015;364(1):8-16. doi:10.1016/j.canlet.2015.04.003.

11. Lord CJ, Ashworth A. The DNA damage response and cancer therapy. *Nature*. 2012;481(7381):287-294. doi:10.1038/nature10760.

12. Lord CJ, Ashworth A. PARP inhibitors: Synthetic lethality in the clinic. *Science*. 2017;355(6330):1152-1158. doi:10.1126/science.aam7344.

13. Lee J-M, Ledermann JA, Kohn EC. PARP Inhibitors for BRCA1/2 mutation-associated and BRCA-like malignancies. *Ann Oncol*. 2014;25(1):32-40. doi:10.1093/annonc/mdt384.

14. Golan T, Kanji ZS, Epelbaum R, et al. Overall survival and clinical characteristics of pancreatic cancer in BRCA mutation carriers. *Br J Cancer*. 2014;111(6):1132-1138. doi:10.1038/bjc.2014.418.

15. Rebelatto TF, Falavigna M, Pozzari M, et al. Should platinum-based chemotherapy be preferred for germline BReast CAncer genes (BRCA) 1 and 2-mutated pancreatic ductal adenocarcinoma (PDAC) patients? A systematic review and meta-analysis. *Cancer Treat Rev*. 2019;80:101895. doi:10.1016/j.ctrv.2019.101895.

16. Pishvaian MJ, Blais EM, Brody JR, et al. Outcomes in Patients With Pancreatic Adenocarcinoma With Genetic Mutations in DNA Damage Response Pathways: Results From the Know Your Tumor Program. *JCO Precision Oncology*. 2019;(3):1-10. doi:10.1200/PO.19.00115.

17. Golan T, Hammel P, Reni M, et al. Maintenance Olaparib for Germline BRCA-Mutated Metastatic Pancreatic Cancer. *N Engl J Med*. 2019;381(4):317-327. doi:10.1056/NEJMoa1903387.

18. Maxwell KN, Wubbenhorst B, Wenz BM, et al. BRCA locus-specific loss of heterozygosity in germline BRCA1 and BRCA2 carriers. *Nat Commun*. 2017;8(1):319. doi:10.1038/s41467-017-00388-9.

19. Patch A-M, Christie EL, Etemadmoghadam D, et al. Whole-genome characterization of chemoresistant ovarian cancer. *Nature*. 2015;521(7553):489-494. doi:10.1038/nature14410.

20. Sakai W, Swisher EM, Karlan BY, et al. Secondary mutations as a mechanism of cisplatin resistance in BRCA2-mutated cancers. *Nature*. 2008;451(7182):1116-1120. doi:10.1038/nature06633.

21. Norquist B, Wurz KA, Pennil CC, et al. Secondary somatic mutations restoring BRCA1/2 predict chemotherapy resistance in hereditary ovarian carcinomas. *J Clin Oncol*. 2011;29(22):3008-3015. doi:10.1200/JCO.2010.34.2980.

22. Polak P, Kim J, Braunstein LZ, et al. A mutational signature reveals alterations

underlying deficient homologous recombination repair in breast cancer. *Nat Genet*. 2017;49(10):1476-1486. doi:10.1038/ng.3934.

23. Aung KL, Fischer SE, Denroche RE, et al. Genomics-Driven Precision Medicine for Advanced Pancreatic Cancer: Early Results from the COMPASS Trial. *Clinical Cancer Research*. 2018;24(6):1344-1354. doi:10.1158/1078-0432.CCR-17-2994.

24. Ersek JL, Black LJ, Thompson MA, Kim ES. Implementing Precision Medicine Programs and Clinical Trials in the Community-Based Oncology Practice: Barriers and Best Practices. *Am Soc Clin Oncol Educ Book*. 2018;38(38):188-196. doi:10.1200/EDBK_200633.

25. Garralda E, Dienstmann R, Piris-Giménez A, Braña I, Rodon J, Tabernero J. New clinical trial designs in the era of precision medicine. *Molecular Oncology*. 2019;13(3):549-557. doi:10.1002/1878-0261.12465.

26. Tempero MA. NCCN Guidelines Updates: Pancreatic Cancer. *J Natl Compr Canc Netw*. 2019;17(5.5):603-605. doi:10.6004/jnccn.2019.5007.

27. Coleman RL, Oza AM, Lorusso D, et al. Rucaparib maintenance treatment for recurrent ovarian carcinoma after response to platinum therapy (ARIEL3): a randomised, double-blind, placebo-controlled, phase 3 trial. *Lancet*. 2017;390(10106):1949-1961. doi:10.1016/S0140-6736(17)32440-6.

28. Telli ML, Timms KM, Reid J, et al. Homologous Recombination Deficiency (HRD) Score Predicts Response to Platinum-Containing Neoadjuvant Chemotherapy in Patients with Triple-Negative Breast Cancer. *Clinical Cancer Research*. 2016;22(15):3764-3773. doi:10.1158/1078-0432.CCR-15-2477.

29. Lee AJX, Endesfelder D, Rowan AJ, et al. Chromosomal instability confers intrinsic multidrug resistance. *Cancer Res*. 2011;71(5):1858-1870. doi:10.1158/0008-5472.CAN-10-3604.

30. Passerini V, Ozeri-Galai E, de Pagter MS, et al. The presence of extra chromosomes leads to genomic instability. *Nat Commun*. 2016;7(1):10754–12. doi:10.1038/ncomms10754.

31. Barber LJ, Rosa Rosa JM, Kozarewa I, et al. Comprehensive genomic analysis of a BRCA2 deficient human pancreatic cancer. Oshima R, ed. *PLoS ONE*. 2011;6(7):e21639. doi:10.1371/journal.pone.0021639.

32. Martinelli P, Carrillo-de Santa Pau E, Cox T, et al. GATA6 regulates EMT and tumour dissemination, and is a marker of response to adjuvant chemotherapy in pancreatic cancer. *Gut*. 2017;66(9):1665-1676. doi:10.1136/gutjnl-2015-311256.

33. Castroviejo-Bermejo M, Cruz C, Llop-Guevara A, et al. A RAD51 assay feasible in

routine tumor samples calls PARP inhibitor response beyond BRCA mutation. *EMBO Mol Med*. 2018;10(12):e9172. doi:10.15252/emmm.201809172.

34. Cruz C, Castroviejo-Bermejo M, Gutiérrez-Enríquez S, et al. RAD51 foci as a functional biomarker of homologous recombination repair and PARP inhibitor resistance in germline BRCA-mutated breast cancer. *Ann Oncol*. 2018;29(5):1203-1210. doi:10.1093/annonc/mdy099.

35. Connor AA, Denroche RE, Jang GH, et al. Association of Distinct Mutational Signatures With Correlates of Increased Immune Activity in Pancreatic Ductal Adenocarcinoma. *JAMA Oncol*. 2017;3(6):774-783. doi:10.1001/jamaoncol.2016.3916.

36. Strickland KC, Howitt BE, Shukla SA, et al. Association and prognostic significance of BRCA1/2-mutation status with neoantigen load, number of tumor-infiltrating lymphocytes and expression of PD-1/PD-L1 in high grade serous ovarian cancer. *Oncotarget*. 2016;7(12):13587-13598. doi:10.18632/oncotarget.7277.

37. Gilmore E, McCabe N, Kennedy RD, Parkes EE. DNA Repair Deficiency in Breast Cancer: Opportunities for Immunotherapy. *J Oncol*. 2019;2019(12):4325105-4325114. doi:10.1155/2019/4325105.

38. Denroche RE, Mullen L, Timms L, et al. A cancer cell-line titration series for evaluating somatic classification. *BMC Res Notes*. 2015;8(1):823–10. doi:10.1186/s13104-015-1803-7.

39. Davies H, Glodzik D, Morganella S, et al. HRDetect is a predictor of BRCA1 and BRCA2 deficiency based on mutational signatures. *Nat Med*. 2017;23(4):517-525. doi:10.1038/nm.4292.

40. Alexandrov LB, Nik-Zainal S, Wedge DC, et al. Signatures of mutational processes in human cancer. *Nature*. 2013;500(7463):415-421. doi:10.1038/nature12477.

41. Bolger AM, Lohse M, Usadel B. Trimmomatic: a flexible trimmer for Illumina sequence data. *Bioinformatics*. 2014;30(15):2114-2120. doi:10.1093/bioinformatics/btu170.

42. Dobin A, Davis CA, Schlesinger F, et al. STAR: ultrafast universal RNA-seq aligner. *Bioinformatics*. 2013;29(1):15-21. doi:10.1093/bioinformatics/bts635.

43. Ahdesmäki MJ, Gray SR, Johnson JH, Lai Z. Disambiguate: An open-source application for disambiguating two species in next generation sequencing data from grafted samples. *F1000Res*. 2016;5(2741):2741. doi:10.12688/f1000research.10082.2.

44. Anders S, Pyl PT, Huber W. HTSeq--a Python framework to work with high-throughput sequencing data. *Bioinformatics*. 2015;31(2):166-169. doi:10.1093/bioinformatics/btu638.

45. Robinson MD, McCarthy DJ, Smyth GK. edgeR: a Bioconductor package for differential expression analysis of digital gene expression data. *Bioinformatics*. 2010;26(1):139-140. doi:10.1093/bioinformatics/btp616.

46. Ritchie ME, Phipson B, Wu D, et al. limma powers differential expression analyses for RNA-sequencing and microarray studies. *Nucleic Acids Res*. 2015;43(7):e47-e47. doi:10.1093/nar/gkv007.

47. Agorku DJ, Tomiuk S, Klingner K, et al. Depletion of Mouse Cells from Human Tumor Xenografts Significantly Improves Downstream Analysis of Target Cells. *J Vis Exp*. 2016;(113). doi:10.3791/54259.

48. Nunez R. DNA measurement and cell cycle analysis by flow cytometry. *Curr Issues Mol Biol*. 2001;3(3):67-70.

49. Van Loo P, Nordgard SH, Lingjærde OC, et al. Allele-specific copy number analysis of tumors. *Proc Natl Acad Sci USA*. 2010;107(39):16910-16915. doi:10.1073/pnas.1009843107.

Author contributions

Yifan Wang, MD (Conceptualization: Lead; Data curation: Lead; Formal analysis: Lead; Investigation: Lead; Methodology: Lead; Project administration: Lead; Visualization: Lead; Writing – original draft: Lead)
Jin Yong Patrick Park, MSc (Conceptualization: Equal; Investigation: Equal; Methodology: Equal; Writing – review & editing: Supporting)
Alain Pacis, PhD (Formal analysis: Equal; Methodology: Equal; Visualization: Equal; Writing – review & editing: Equal)
Robert E Denroche, MSc (Data curation: Equal; Formal analysis: Equal; Methodology: Equal; Visualization: Equal; Writing – review & editing: Equal)
Gun Ho Jang, PhD (Data curation: Equal; Formal analysis: Equal; Methodology: Equal; Writing – review & editing: Equal)
Amy Zhang, MSc (Data curation: Equal; Formal analysis: Equal; Methodology: Equal; Visualization: Equal; Writing – review & editing: Equal)
Adeline Cuggia, MSc (Data curation: Equal; Formal analysis: Equal; Methodology: Equal; Writing – review & editing: Equal)
Celine Domecq, MSc (Data curation: Equal; Formal analysis: Equal; Investigation: Equal; Methodology: Equal; Writing – review & editing: Equal)
Jean Monlong, PhD (Formal analysis: Equal; Investigation: Equal; Methodology: Equal; Visualization: Equal; Writing – review & editing: Equal)
Maria Raitses-Gurevich, PhD (Data curation: Equal; Formal analysis: Equal; Resources: Equal; Writing – review & editing: Equal)
Robert C Grant, MD (Methodology: Equal; Writing – review & editing: Equal)
Ayelet Borgida, MSc (Methodology: Equal; Resources: Equal; Writing – review & editing: Equal)
Spring Holter, MSc (Methodology: Equal; Resources: Equal; Writing – review & editing: Equal)
Chani Stossel, MSc (Methodology: Equal; Resources: Equal; Writing – review & editing: Equal)
Simeng Bu, BSc (Data curation: Equal; Investigation: Equal; Methodology: Equal; Writing – review & editing: Equal)
Mehdi Masoomian, MD (Investigation: Equal; Methodology: Equal; Writing – review & editing: Equal)
Ilinca Lungu, MSc (Investigation: Equal; Methodology: Equal; Resources: Equal; Writing – review & editing: Equal)
John Bartlett, PhD (Investigation: Equal; Methodology: Equal; Resources: Equal; Writing – review & editing: Equal)
Julie Wilson, PhD (Funding acquisition: Equal; Resources: Equal; Writing – review & editing: Equal)
Zu-Hua Gao, MD, PhD (Data curation: Equal; Investigation: Equal; Methodology: Equal; Resources: Equal; Writing – review & editing: Equal)
Yasser Riazalhosseini, PhD (Funding acquisition: Equal; Investigation: Equal; Methodology: Equal; Supervision: Equal; Writing – review & editing: Equal)

Jamil Asselah, MD (Resources: Equal; Writing – review & editing: Equal)
Nathaniel Bouganim, MD (Resources: Equal; Writing – review & editing: Equal)
Tatiana Cabrera, MD (Resources: Equal; Writing – review & editing: Equal)
Louis-Martin Boucher, MD, PhD (Resources: Equal; Writing – review & editing: Equal)
David Valenti, MD (Resources: Equal; Writing – review & editing: Equal)
James Biagi, MD, MASc (Resources: Equal; Writing – review & editing: Equal)
Celia MT Greenwood, PhD (Methodology: Equal; Supervision: Equal; Writing – review & editing: Equal)
Paz Polak, PhD (Resources: Equal; Supervision: Equal; Writing – review & editing: Equal)
William D Foulkes, MBBS, PhD (Resources: Equal; Supervision: Equal; Writing – review & editing: Equal)
Talia Golan, MD (Funding acquisition: Equal; Resources: Equal; Supervision: Equal; Writing – review & editing: Equal)
Grainne O'Kane, MD (Data curation: Equal; Formal analysis: Equal; Methodology: Equal; Resources: Equal; Writing – review & editing: Equal)
Sandra E Fischer, MD (Investigation: Equal; Methodology: Equal; Resources: Equal; Writing – review & editing: Equal)
Jennifer J Knox, MD, MSc (Funding acquisition: Equal; Resources: Equal; Supervision: Equal; Writing – review & editing: Equal)
Steven Gallinger, MD, MSc (Conceptualization: Equal; Funding acquisition: Equal; Resources: Equal; Supervision: Equal; Writing – review & editing: Equal)
George Zogopoulos, MD, PhD (Conceptualization: Lead; Formal analysis: Equal; Investigation: Equal; Methodology: Lead; Project administration: Lead; Resources: Lead; Supervision: Lead; Writing – original draft: Equal)

Acknowledgments

We acknowledge the contributions of Crystal Haigh (patient enrolment), HPB Surgical and Medical Oncology, Pathology and Interventional Radiology at the McGill University Health Centre. We also acknowledge the contributions of team members at the Ontario Institute for Cancer Research within the Genomics & Bioinformatics platform (genomics.oicr.on.ca), as well as the contributions of Dianne Chadwick, Sheng-Ben Liang and Sana Sagri at the University Health Network Oncology Biobank.

Funding

This study was supported through funding provided by the Cancer Research Society/Ganotec-Marc-André Pigeon Memorial Fund (Grant #20280), the Terry Fox Research Institute (Project #1078) and the Pancreatic Cancer Canada Foundation (PancONE™). This study was conducted with the support of the Ontario Institute for Cancer Research (PanCuRx Translational Research Initiative) through funding provided by the Government of Ontario, the Wallace McCain Centre for Pancreatic Cancer supported by the Princess Margaret Cancer Foundation and the Canadian Cancer Society Research Institute. The study was also supported by charitable donations from the Canadian Friends of the Hebrew University (Alex U. Soyka). Y.W. is supported by a Vanier Canada Graduate Scholarship, the Fonds de recherche du Québec – Santé/Ministère de la Santé et des Services sociaux training program, and the McGill University Surgical-Scientist Program. Y.R. is a research scholar of the Fonds de recherche du Québec – Santé. G.O.K. is supported by the Lewitt fellowship. J.K. is the recipient of the Wilfred G. Lewitt Chair in Pancreatic Cancer Research. S.G. is the recipient of an Investigator Award from the Ontario Institute for Cancer Research. G.Z. is a clinical research scholar of the Fonds de recherche du Québec – Santé.